THESIS FOR THE DEGREE OF LICENTIATE OF ENGINEERING

Microresonator combs for coherent optical communications

ATTILA FÜLÖP

CHALMERS

Photonics Laboratory
Department of Microtechnology and Nanoscience – MC2
CHALMERS UNIVERSITY OF TECHNOLOGY

Göteborg, Sweden 2016

Microresonator combs for coherent optical communications
ATTILA FÜLÖP

Chalmers University of Technology
Department of Microtechnology and Nanoscience – MC2
Photonics Laboratory
SE-412 96 Göteborg, Sweden
Telephone: +46 (0)31-772 1000

ISSN 1652-0769
Technical Report MC2-344

Cover:
Sketch of a microresonator frequency comb with multicolored output.

Chalmers Reproservice
Göteborg, Sweden 2016

Microresonator combs for coherent optical communications
Thesis for the degree of Licentiate of Engineering
ATTILA FÜLÖP
Department of Microtechnology and Nanoscience – MC2
Photonics Laboratory
Chalmers University of Technology

Abstract

This thesis covers the study of microresonator-based optical frequency combs for use in coherent optical communication links. Current links typically utilize several free-running lasers to achieve wavelength-division multiplexing (WDM). Having an integrated frequency comb as a source instead could potentially simplify the transmitter while at the same time open up new possibilities on the digital signal processing (DSP) side in the receiver.

The thesis goes into some detail to describe what requirements there are on the combs to be useful for this application. Specifically the power per line and related flatness is analyzed. Additionally a large part of the thesis is dedicated to describe the working principle of microresonators. The linear low-power regime is described in detail while a simple Lugiato-Lefever model is analyzed for the nonlinear high-power regime.

The appended papers describe two different microresonators with different initialization mechanisms; one where the dispersion is locally tuned using higher order modal interactions while the second one is seeded with three coherent pump waves. The first paper demonstrates that such combs fulfill the criteria for being light sources in long-haul communication systems. This is demonstrated by using it to send data over a more than 6000 km long transmission link.

Keywords: Fiber-optic communication, integrated optics devices, nonlinear optics, four-wave mixing, microresonators.

Sammanfattning

Denna avhandling handlar om mikroresonatorbaserade optiska frekvenskammar för användning i koherenta optiska kommunikationslänkar. Dagens länkar använder typiskt flera frigående lasrar för att kunna skicka data med våglängdsmultiplicering. Skulle man ha tillgång till en frekvenskam på en integrerad krets istället, skulle man kunna förenkla delar av sändaren samtidigt som nya möjligheter för optimering i den digitala signalbehandlingen i mottagaren skulle bli tillgängliga.

Avhandligen beskriver krav som denna frekvenskam måste uppfylla för att kunna användas i kommunikationssammanhang. Den analyserar speciellt kraven på optisk effekt i de tillgängliga linjerna och den relaterade totala effektvariationen i kammen. Avhandligen innehåller dessutom en beskrivning av mikrokammarnas fysikaliska beteende. Den linjära delen, där den optiska effekten är låg, beskrivs i detalj, medan den icke-linjära regimen, den med hög optisk effekt, analyseras genom en förenklad Lugiato-Lefever-modell.

De bifogade artiklarna beskriver två olika mikroresonatorer med olika initieringsmekanismer; en där dispersionen är inställd med hjälp av interaktioner mellan högre ordningens moder samt en som är initierad med tre koherenta pumpvågor. Artikel nummer ett demonstrerar dessutom att sådana kammar uppfyller kraven för optisk kommunikation över långa avstånd. Detta visas genom att sända data med hjälp av kamlinjerna över en mer än 6000 km lång länk.

Kivonat

Ez a tézis mikrorezonátor-alapú optikai frekvenciafésűkről szól amelyek koherens optikai kommunikációra használhatóak. A mai összeköttetések tipikusan több darab szabadon működő lézert használnak a hullámhossz-osztásos multiplexeléshez. Egy integrált áramkörön levő frekvenciafésű le tudná egyszerűsíteni az adót és egyszerre lehetővé tudna tenni a vevőnél futó digitális jelfeldolgozásban újabb funkciókat.

A tézis leír követelményeket amiknek a fésűnek meg kell felelnie a kommunikációban való használathoz. Elemzi különösen az optikai intenzitásra és a fésű egyenletességére való elvárásokat. Ezen kívűl leírja a mikrorezonátorok fizikai működését a lineáris, alacsony optikai intenzitású módban is meg egy leegyszerűsített Lugiato-Lefever model alapján a nemlineáris, magas optikai intenzitású módban is.

A csatolt cikkek két különböző indítású mikrorezonátort használnak: az első a magassabb rendű módok által beállított diszperzió segítségével indúlt míg a második három koherens pumpa által indúlt. Az első cikk ezen kívűl bemutatja hogy ezek a fésűk megfelelnek a hosszú távú kommunikációhoz kapcsolt követelményeknek: több mint 6000 km távolságon át való adatküldést mutat be.

Acknowledgements

First of all, I would like to thank my supervisor, Associate Prof. Victor Torres-Company, without his continuing support and knowledge I would not have made it this far. I would additionally also like to thank my examiner Prof. Peter Andrekson for discussions and lab support and Prof. Magnus Karlsson for discussions and teaching of the relevant topics.

I would also like to thank and acknowledge Pei-Hsun Wang, Abdullah Al Noman and Prof. Andrew Weiner as well as the rest of the ultrafast optics laboratory at Purdue University for the supplied ring resonators and the great support and kindness I received when visiting.

Moreover I would like to thank all the members of the photonics laboratory here at Chalmers. Specifically I would like to thank Clemens Krückel both for great discussions on nonlinear optics and organizing out-of office trips and Emanuel Haglund for our friendship during our whole Chalmers education. I would like to thank Dr. Erik Haglund for being a great office mate and Dr. Krzysztof Szczerba, Lars Lundberg and Dr. Vicente Durán Bosch for great discussions on various topics. Additionally I would like to acknowledge Dr. Tobias Eriksson, Abel Lorences Riesgo and Mikael Mazur for being very helpful in the lab and with related discussions.

Last, but not least, I would like to thank all of my family and friends for being supportive and joyful to be around.

List of Papers

This thesis is based on the following appended papers:

[A] **A. Fülöp**, M. Mazur, T. A. Eriksson, P. A. Andrekson, V. Torres-Company, P.-H. Wang, Y. Xuan, D. E. Leaird, M. Qi, and A. M. Weiner, "Long-haul coherent transmission using a silicon nitride microresonator-based frequency comb as WDM source," *Conference on lasers and electro-optics (CLEO)*, San Jose, USA, paper SM4F.2, 2016.

[B] **A. Fülöp**, C. J. Krückel, D. Castelló-Lurbe, E. Silvestre, and V. Torres-Company, "Triply resonant coherent four-wave mixing in silicon nitride microresonators," *Optics Letters*, vol. 40, no. 17, pp. 4006-4009, 2015.

Related publications and conference contributions by the author, not included in the thesis:

[C] C. J. Krückel, **A. Fülöp**, P. A. Andrekson, and V. Torres-Company, "Continuous-wave nonlinear optics in low-stress silicon nitride waveguides," *Optical Fiber Communication Conference (OFC)*, Los Angeles, USA, paper W1K.4, 2015.

[D] **A. Fülöp**, C. J. Krückel, D. Castelló-Lurbe, E. Silvestre, and V. Torres-Company, "Phase-sensitive resonant four-wave mixing in silicon nitride microresonators," *Conference on Lasers and Electro-Optics (CLEO) Europe*, Munich, Germany, paper CD_P_9, 2015.

[E] A. Lorences-Riesgo, T. A. Eriksson, **A. Fülöp**, M. Karlsson, and P. A. Andrekson, "Frequency-comb regeneration for self-homodyne superchannels," *European Conference and Exhibition on Cptical Communication (ECOC)*, Valencia, Spain, paper We.3.6.2., 2015.

[F] C. J. Krückel, **A. Fülöp**, T. Klintberg, J. Bengtsson, P. A. Andrekson, and V. Torres-Company, "Linear and nonlinear characterization of low-stress high-confinement silicon-rich nitride waveguides," *Optics Express*, vol. 23, no. 20, pp. 25827-25837, 2015.

[G] A. Lorences-Riesgo, T. A. Eriksson, **A. Fülöp**, P. A. Andrekson, and M. Karlsson, "Frequency-comb regeneration for self-homodyne superchannels," *Journal of Lightwave Technology*, vol. 34, no. 8, pp. 1800-1806, 2016.

[H] M. Rezagholipour Dizaji, C. J. Krückel, **A. Fülöp**, P. A. Andrekson, V. Torres-Company, and L. R. Chen, "Cross-phase-modulation-based wavelength conversion in low-stress silicon-rich nitride waveguide," *Optical Fiber Communication Conference (OFC)*, Anaheim, USA, paper Tu2K.4, 2016.

[I] X. Liu, M. Pu, B. Zhou, C. J. Krückel, **A. Fülöp**, V. Torres-Company, and M. Bache, "Octave-spanning supercontinuum generation in a silicon-rich nitride waveguide," *Optics Letters*, vol. 41, no. 12, pp. 2719-2722, 2016.

[J] X. Liu, M. Pu, B. Zhou, C. J. Krückel, **A. Fülöp**, V. Torres-Company, and M. Bache, "Octave-spanning supercontinuum generation in a silicon-rich nitride waveguide," *Conference on Lasers and Electro-Optics (CLEO)*, San Jose, USA, paper SW1Q.3, 2016.

Abbreviations

AWG arrayed waveguide grating.
BER bit error rate.
CMOS complimentary metal-oxide-semiconductor.
CW continuous-wave.
DSP digital signal processing.
EDFA erbium-doped fiber amplifier.
FSR free spectral range.
FWHM full width at half maximum.
FWM four-wave mixing.
HNLF highly nonlinear fiber.
LO local oscillator.
NLSE nonlinear Schrödinger equation.
OSNR optical signal-to-noise ratio.
RF radio frequency.
WDM wavelength-division multiplexing.

Contents

Abstract i

Sammanfattning ii

Kivonat iii

Acknowledgements v

List of Papers vii

Abbreviations ix

1 Introduction 1
- 1.1 Optical frequency combs . . . 2
  - 1.1.1 Comb implementation . . . 3
- 1.2 This thesis . . . 4

2 Combs for communication 5
- 2.1 Previous demonstrations . . . 5
- 2.2 Integration . . . 6

3 Comb requirements 9
- 3.1 Coherent detection . . . 9
  - 3.1.1 Optical signal-to-noise ratio . . . 10
  - 3.1.2 Phase noise . . . 10
- 3.2 Comb details . . . 12
  - 3.2.1 Power parameters . . . 12

4 Microresonator physics **17**
4.1 The linear regime 17
4.1.1 The coupling region 19
4.1.2 Characterizing the linear parameters 20
4.2 Light propagation and the Kerr effect 21
4.3 The Lugiato-Lefever equation 22
4.4 Comb initialization 24
4.4.1 Soliton generation 26
4.4.2 The normal dispersion regime 27
4.5 Noise properties 27
4.6 Other practical considerations 28
4.6.1 The temperature 28
4.6.2 Conversion efficiency and the drop port 30

5 Future outlook **31**

6 Summary of papers **33**

References **34**

Papers **47**

Chapter 1

Introduction

The need to communicate and send messages between people has existed since the invention of the written word. For most of the history of humankind this has involved sending messages by carrier, either humans or carrier animals. While there are modern suggestions for carrying internet protocol packets using avian carriers [1], the vast majority of data traffic has been transmitted on lower-latency links for the past century. The first transatlantic telegraph cable was able transmit a letter from Queen Victoria in just above one hour. By comparison, modern fiber-optic cables carry several terabits of data each second. The need for cheap and reliable transmission capacity, both over short and long distances, is however expected to keep increasing for the foreseeable future, motivating the need for ever-higher performing and more efficient ways of data transmission.

Fiber-optic technologies have been rapidly replacing electrical connections on shorter and shorter distances, from the transcontinental down to links of only a few meters in length. Key enabling technologies for this have been the laser [2] and the optical fiber [3]. More recently the erbium-doped fiber amplifier (EDFA) [4] has enabled data transmission over long distances without the need for repeater stations. The EDFA has the ability to amplify optical signals across a wide bandwidth around $\lambda = 1550\,\mathrm{nm}$. The availability of a wide transmission window gave rise to the concept of wavelength-division multiplexing (WDM), where several communication channels could be transmitted in parallel over different wavelengths.

This naturally leads to the question of how the light sources can adapt. In today's commercial systems, this typically means that there is a wide array of free-running lasers operating at slightly different wavelengths which are then

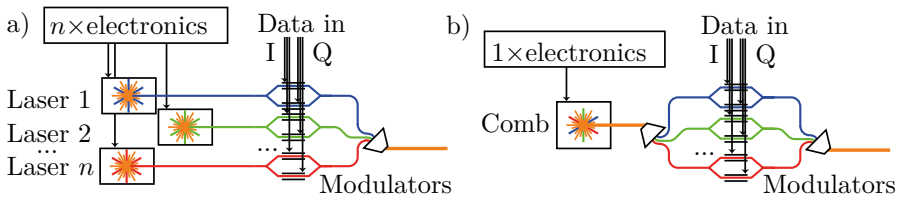

Figure 1.1. a) Sketch showing a transmitter setup with several free-running lasers connected to modulators. b) The same setup where the lasers have been replaced by a single frequency comb source.

modulated with data and combined before being transmitted over the link. What if there was a light source that simultaneously produced light at several different wavelengths and that could be integrated on a single chip together with the data modulators? There is, it is called an optical frequency comb, figure 1.1 shows a sketch indicating the practical difference between the two situations.

1.1 Optical frequency combs

Frequency combs in general are coherent light sources where the components at different wavelengths are evenly spaced in frequency and are phase-locked with respect to each other. Looking at it from the time domain, this looks like pulses with a repetition rate corresponding to the frequency spacing of its lines. The first demonstrated laser-based frequency combs were the actively mode locked lasers [5, 6]. The field has however grown rather quickly since then. In 2000, combs spanning more than an octave of bandwidth, permitting frequency self-referencing through the use of second harmonic generation were demonstrated [7–12]. In 2005, this yielded a part of the Nobel prize in physics.

Optical frequency combs have been demonstrated to allow advances for a wide spectrum of applications. Self-referenced combs enable and significantly simplify optical clocks. These permit measuring optical frequencies with the accuracy of radio frequency (RF) references such as the Cesium standard. The usage of combs as rulers, against which calibrations can be made, extends into several fields of spectroscopy. It has been demonstrably useful in both molecular spectroscopy [13–16] and astronomy [17, 18] reaching all the way to attosecond scale measurements [19]. Even spectroscopic measurements that

need to be done outside the laboratory, potentially in a moving vehicle, have been shown to be possible using femtosecond laser-based combs [20].

In another measurement context, combs have also been used for precise distance measurements on the nanometer scale using both time-of-flight [21] as well as interferometric [22, 23] techniques.

For potentially faster and in some cases simpler spectroscopic and interferometric measurement applications, recently there have been developments in dual-comb spectroscopy. In that setup two combs with slightly different repetition rates are mixed together on a photodiode with one of the combs having passed through a measurement sample [24–27]. As long as a measurement resolution equal to the comb spacing is satisfactory, this can give information about both the amplitude and the phase response of a measured sample.

Using a comb in the opposite direction, when an absolute RF frequency reference is not available, a laser can be locked to an optical cavity resonance. Generating a self-referenced comb from this line and feeding it into a photodetector can provide a RF source with phase noise properties beyond what is possible using conventional means [28]. This can potentially lead to new categories of integrated low-noise RF sources. Even without self-referencing, a stable frequency comb can provide low phase noise RF sources [29, 30].

Since the lines of a frequency comb are coherent with respect to each other, adjusting their relative phases and amplitudes gives precise control over how the optical field looks in the time domain. Thus, combining a frequency comb with pulse shaping optics, one can implement arbitrary waveform generation [31, 32].

Last, but not least, Kerr frequency combs have also been used to generate entangled photons for quantum optical applications such as quantum computation and communication [33]. Since these combs are based on integrated technology, they have the potential of enabling more easily scalable quantum computing devices.

1.1.1 Comb implementation

The comb implementations significantly depend on the actual use cases [34]. For the use of optical clocks and references, absolute frequency precision is needed, requiring combs that span more than an octave of bandwidth that can be stabilized to themselves [12]. In other cases, such as the ones discussed here later, compactness and robustness is more important, with self-referencing not being necessary at all. It should be mentioned however, that semi-compact femtosecond mode-locked lasers with highly nonlinear fiber (HNLF)-based broadening have been demonstrated as well recently [35].

Not only mode-locked lasers can generate frequency combs though. They can be generated through the use of cascaded electro-optic phase modulators as well [36]. This platform has the convenient property that the central wavelength and the line spacing can be tuned individually by shifting the pump laser or the RF-clock respectively. By applying nonlinear broadening in for example a HNLF, these systems can be extended to cover a broad bandwidth as well [37] all the way to octave-spanning [38].

Moving towards the most compact sources, we arrive at the main focus of this thesis: the microresonators [39]. In 2007, comb generation using whispering-gallery mode resonators consisting of silica-based toroidal microcavities were demonstrated [40]. Following that, comb generation using microresonators has been demonstrated in a wide variety of material platforms including CaF_2 [41, 42] and MgF_2[43] crystalline resonators, diamond resonators [44], silica wedge-resonators [45], doped silica (Hydex™) rings [46], silicon rings [47], aluminium nitride rings [48], and silicon nitride microresonators [49–52]. The working principle of these devices is the nonlinear Kerr effect [53]. They are usually pumped with a single or very few high-powered laser lines, which then through four-wave mixing cascade into a full comb. Inside the resonators themselves, this manifests itself as a circulating pulse profile that can consist of both bright solitons [54] and dark pulses [55].

1.2 This thesis

The focus of this thesis will be to connect the concept of coherent communication with that of frequency comb generation in microresonators. In chapter 2, the microresonator combs and their potential uses and advantages in optical communications is discussed. Chapter 3 starts by briefly describing the relevant building blocks of a coherent communication system. It later goes a bit deeper into what this translates to in terms of requirements and limits for a comb-based light source. Chapter 4 then goes into more technical detail about the working principles and possible modeling of the microresonators themselves.

Chapter 2

Combs for communication

The previous chapter introduced the concept of optical frequency combs and mentioned that there are microresonator-based ones that might work well for using in optical communications. This chapter will discuss the possibilities and advantages of these systems.

2.1 Previous demonstrations

The most obvious way to implement comb sources in a communications setup is to use them as drop-in replacements for the lasers in a WDM data source. This enables using a single laser to seed all communication channels simultaneously simplifying both the physical setup, but also permitting potentially higher requirements on the laser itself. Cumulative data rates above a terabit have been shown in this way using electro-optic combs with [56] and without [57] external broadening as well as microresonator-based [58, 59] frequency combs. Extending this concept to multiple cores in a multi-core fiber using a broadened electro-optic comb have allowed demonstrations of petabit rates [60].

Additional advantages can be had by also utilizing the mutual coherence of the comb lines. The nonlinear Kerr effect in fibers is a deterministic impairment that depends on the channel power and spacing. In a comb-based multi-channel transmitter, both the exact frequency differences between the channels and the data is known. This way one can pre-distort the data in a way such that the nonlinearities in the transmission link are cancelled out by the time the packets reach the receiver [61]. Experiments have shown that using this technique, one can at least double the permitted transmission distance [62].

From a total system perspective, using a single laser as a source for multiple WDM channels can also cut the power consumption requirements for the transmitter, see figure 1.1 for a basic sketch. To generate N laser lines with free running lasers, one needs N diode controllers and N temperature controllers. Using an electro-optic comb this can be replaced by a single diode controller, a single temperature controller, RF electronics (clock source, RF amplifiers and modulator bias) and an EDFA. For an integrated comb source the amount of power consuming electronics is reduced further. In the case of a microresonator based comb one needs a single diode controller and temperature controller for the pump laser, one or potentially two EDFAs and a temperature controller for the chip. Assuming a controller power consumption of around 10 W and an EDFA power consumption of 50 W one starts saving electrical power already after 12 lines compared with the free running lasers.

2.2 Integration

For comb generation on a chip, there are several options available. Apart from the previously mentioned microresonators, there have been demonstrations of electro-optic combs [63], passively mode-locked lasers [64], and quantum-dash mode-locked lasers [65]. The material in these examples was InP, which permits DFB lasers, modulators and other active components to be integrated as well [66]. Other material platforms include Si, SiO_2 and SiN [67]. While lasers are not available here, they have the potential to be complimentary metal-oxide-semiconductor (CMOS) compatible allowing integration of other electronics on the same chip.

Apart from the CMOS compatibility, microresonator based combs using these materials have some additional nice properties. They naturally offer a way of designing their comb spacing by changing the resonator length to potentially match the standard ITU grid [68]. By designing their cross sections, one also maintain control over their dispersion and nonlinear properties, which will become important as will be discussed in section 4.4. The requirements for the comb generation is basically that the material should have good power handling capabilities and a high nonlinear index. Silicon nitride is a good material candidate due to the combination of relatively high nonlinear index and, as opposed to silicon which has an even higher nonlinear index, a lack of two-photon absorption in the telecommunications band.

To make full use of the integration possibilities, one would want to integrate them on the same chip as other components, both active and passive, such as modulators and couplers. This avoids having to couple the light in and out of

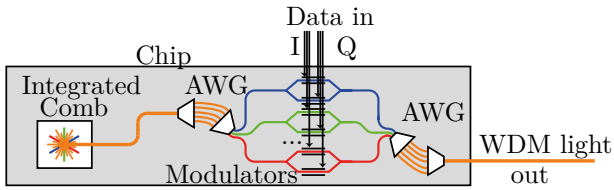

Figure 2.1. A sketch showing the idea of a fully integrated WDM transmitter. The optical frequency comb that gets generated is sent to an arrayed waveguide grating (AWG) that splits the lines into different waveguides, those are then modulated using IQ modulators and then recombined using a second AWG. Out from the chip there is a single waveguide containing a fully modulated WDM spectrum.

the chip more times than necessary, ideally using only a single output coupler. Figure 2.1 displays this concept. Having access to such a fully integrated device could enable higher bandwidth communication channels for shorter distances also, where a full array of free-running lasers are not feasible. On the receiver side, a similar approach could be used for the local oscillators (LOs) in the coherent receiver maintaining the coherence between the channels for the digital signal processing (DSP).

Chapter 3

Comb requirements

This chapter is intended to look at combs and their requirements from the usage side, specifically asking the question: how does a comb have to behave to be useful in a coherent communication context?

3.1 Coherent detection

In fiber-optic communications today, the two most common ways to detect data-signals are direct detection and coherent detection. In a direct detection scheme, the receiver essentially consists of a photodetector that responds to the intensity of the incoming light. This method is simple and useful for on-off keying signals. It can however not detect the phase of the incoming light and therefore cannot be used to detect more spectrally efficient formats. In those cases coherent detection is used. In coherent detection schemes, the incoming optical signal is mixed together with a free-running LO in an optical 90° hybrid. At the output of the hybrid, balanced photodetectors are placed from which one can extract the real part of the original optical field as well as the imaginary part, see figure 3.1.

Using DSP, one can then correct for both the frequency and phase offset of the LO as well as apply additional algorithms for compensation of various other signal impairments.

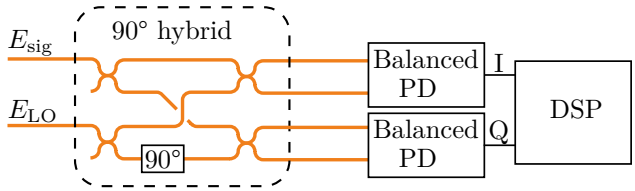

Figure 3.1. A sketch of a single polarization coherent receiver showing the 90° hybrid with the 90° phase shifter and the balanced photodetectors. Extending this to a dual-polarization receiver essentially means putting polarization-beam splitters in front of both the signal and LO input and doubling the rest.

3.1.1 Optical signal-to-noise ratio

On the receiver side, for the DSP to operate well, there are a few requirements though. Perhaps the most important parameters to estimate the final bit error rate (BER) is the optical signal-to-noise ratio (OSNR) at the receiver. The electrical signal-to-noise ratio and the resulting BER for a gray-coded dual-polarization quadrature amplitude modulation signal can be estimated as follows [69]:

$$\text{SNR} = \text{OSNR}\frac{B_{\text{osa}}}{B_{\text{r}}\log_2(M)}, \tag{3.1}$$

$$\text{BER} \approx \frac{2}{\log_2(M)}\left(1-\frac{1}{\sqrt{M}}\right)\text{erfc}\left(\sqrt{\frac{3\log_2(M)}{2(M-1)}\text{SNR}}\right), \tag{3.2}$$

where M is the number of constellation points, B_{r} is the symbol rate of the signal, and B_{osa} is the resolution at which the OSNR was measured, typically this is 12.5 GHz (0.1 nm).

Since the OSNR degrades linearly with the number of amplifiers in the link [70] and the final requirement depends on the chosen modulation format, the exact requirement at the transmitter side will vary from system to system. For example, to receive a perfect 10 GBaud 64QAM signal that is only degraded by additive white Gaussian noise with a BER of 10^{-3} at the receiver side, the OSNR at 0.1 nm resolution should be above 21.6 dB.

3.1.2 Phase noise

Since the data modulation makes use of the phase as well as the amplitude of the light, having too high phase noise will jeopardize the signal quality. The

most simple way to characterize the phase noise of an optical signal is by its optical linewidth. The relevant linewidth in this case, $\Delta\nu$, is the linewidth of the mixing product of the signal and LO laser visible after the 90° hybrid. In the situation where the LO laser is free-running compared to the input signal, this is essentially the sum of the two lasers' individual linewidths: $\Delta\nu = \Delta\nu_{\text{sig}} + \Delta\nu_{\text{LO}}$. It is however worth noting that if the signal has been transmitted over some distance, the dispersion compensation process in the DSP may enhance the phase noise of the incoming signal and thus increase the total effective linewidth [71].

An intuitive way of looking at this is that the coherence time of the laser line cannot be shorter than the symbol duration, T_{s}. Since the linewidth of a laser is essentially the inverse of its coherence time, the relevant metric is thus the dimensionless normalized linewidth $\Delta\nu T_{\text{s}}$. The exact requirement on the size of $\Delta\nu T_{\text{s}}$ will depend on the modulation format that one wishes to use and the amount of penalty in the OSNR requirement one is willing to accept. The choice of phase tracking algorithm will also be of importance [72, 73]. For the example case in the previous subsection, accepting a 1 dB penalty to the OSNR requirement will put the final OSNR requirement at roughly 23 dB with a linewidth requirement around 1 MHz according to ref. [72]. Table 3.1 shows some other example cases with OSNR and combined linewidth requirements at the receiver side.

Modulation format	Symbol rate [GBaud]	OSNR [dB]	Linewidth [kHz]
QPSK	10	9.8	4 100
	40	15.9	16 400
16QAM	10	16.6	1 400
	40	22.6	5 600
64QAM	10	22.6	400
	40	28.6	1 600
256QAM	10	28.5	80
	40	34.5	320

Table 3.1. Table showing the OSNR and combined linewidth requirements for different modulation formats at the receiver. The OSNR value is calculated using equation 3.2 and additionally includes a 1 dB penalty to get a matching linewidth requirement [72].

3.2 Comb details

Given than the comb will be used for data transmission with higher order modulation formats accepting a non-zero BER due to the use of forward error correction, some requirements can now be stated. While the results in table 3.1 show the requirements on the receiver side for a given BER of 10^{-3}, the requirements on the comb itself are somewhat higher. Assuming a single transmission span, that is doubling the number of EDFAs from one after the modulator to two, with the second one after the fiber, increases our required OSNR by 3 dB. We also have to assume that, for higher order modulation formats, there will be an additional implementation penalty from the imperfect equipment, not just the 1 dB included in the table for the phase noise tolerance. Additionally, the OSNR that is measured at the modulator will not directly correspond to the OSNR of the comb itself, unless it is both high-powered and completely flat. Figure 3.2 illustrates the way a typical non-flat comb would be set up in front of the data modulation. If it is flat but low powered, Point 1 would be the location at which the OSNR requirements are placed. If it is not flat though, there will have to be a flattening stage with a programmable filter and a second EDFA before the OSNR measurement point, Point 2.

The following section describes how an OSNR requirement at these points can be translated into power-per-line and flatness requirements for the comb itself. For the purpose of clarity, one high-end example will be considered. To transmit a 40 GBaud 64QAM signal over a single transmission link, table 3.1 shows that for a 1 dB implementation penalty the required OSNR at the receiver would be 28.6 dB, for these formats however a higher implementation penalty needs to be considered owing to imperfect equipment. Assuming instead a 4.4 dB total implementation penalty followed by the 3 dB cost of doubling the number of EDFAs after the modulator, the OSNR requirement after the flattening stage would instead be 35 dB.

3.2.1 Power parameters

For the OSNR criteria to be fulfilled for each line, it is appropriate to specify our requirements in terms of power and noise for the weakest lines. In the case where the comb is followed by a single EDFA, this will provide us with a requirement for the minimum power in each line.

Assuming that the noise is dominated by the amplified spontaneous emission noise added by the amplifier, the signal power, $P_{\mathrm{s,out}}$, and noise power, $P_{\mathrm{n,out}}$,

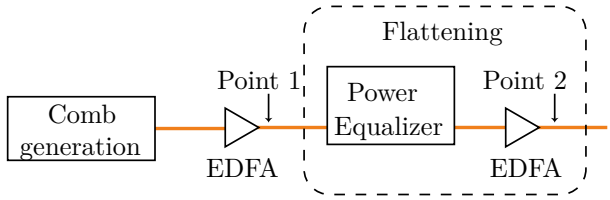

Figure 3.2. A sketch showing the different possible points for OSNR measurement. In the case where the comb is flat enough, the relevant point for OSNR measurement is Point 1, whereas if a flattening stage is required, Point 2 would be the place.

in each comb line after the EDFA, can be written as follows [70]:

$$P_{\mathrm{s,out}} = P_{\mathrm{s}} G, \tag{3.3}$$

$$P_{\mathrm{n,out}} = P_{\mathrm{ASE}} = 2 n_{\mathrm{sp}} h\nu (G-1)\Delta\nu. \tag{3.4}$$

Here, P_{s} is the power per line of the comb coming into the EDFA while G and n_{sp} are the gain and the spontaneous emission factor for the EDFA and h being Planck's constant. The total spontaneous emission factor (meaning both polarizations), $2n_{\mathrm{sp}}$, is equivalent to the noise figure of the EDFA when it is operating in saturation. The signal is assumed to be centered around the frequency ν, while the noise is integrated over a bandwidth $\Delta\nu$.

Assuming that the gain G is large, the OSNR can then be simplified as follows:

$$\begin{aligned} \mathrm{OSNR} &= \frac{P_{\mathrm{s}} G}{2 n_{\mathrm{sp}} h\nu (G-1)\Delta\nu} \\ &\approx \frac{P_{\mathrm{s}}}{2 n_{\mathrm{sp}} h\nu \Delta\nu}. \end{aligned} \tag{3.5}$$

This gives a requirement for the input power of each line in the comb:

$$P_{\mathrm{s,min}} = \mathrm{OSNR}_{\mathrm{req}} 2 n_{\mathrm{sp}} h\nu \Delta\nu. \tag{3.6}$$

At $\lambda = 1550\,\mathrm{nm}$, with a resolution of $\Delta\lambda = 0.1\,\mathrm{nm}$ using an EDFA with a noise figure of 5 dB, the 35 dB OSNR requirement translates to a minimum power per line of $-18.0\,\mathrm{dBm}$.

If the comb flatness (i.e. the difference in power between the strongest and weakest peak) is worse than what the application requires, a flattening stage is required. A typical flattening stage would contain a programmable filter

(a pulse shaper) followed by a second EDFA. However, a pulse shaper has a maximum allowed power input per line as well as a non-zero insertion loss [74, 75], this will put a second criterion on the comb lines. We can define the flatness parameter as the power ratio between the strongest and the weakest lines of interest:

$$F = \frac{P_{\mathrm{s,max}}}{P_{\mathrm{s,min}}}. \tag{3.7}$$

Before the flattening stage, one would like to have a variable attenuator (to keep G_1 as high as possible) with attenuation A_1. The flattening stage itself will then have an insertion loss, L, and an attenuation factor for the strongest line, $A_2 = 1/F$. Assuming that the two EDFAs have identical noise figure, we can then write the output powers and OSNRs as:

$$P_{\mathrm{s,out,min}} = P_{\mathrm{s,min}} G_1 A_1 L G_2, \tag{3.8}$$

$$P_{\mathrm{s,out,max}} = P_{\mathrm{s,max}} G_1 A_1 L A_2 G_2 = P_{\mathrm{s,min}} F G_1 A_1 L A_2 G_2 = P_{\mathrm{s,min}} G_1 A_1 L G_2, \tag{3.9}$$

$$P_{\mathrm{n,out,min}} = 2 n_{\mathrm{sp}} h\nu\Delta\nu((G_1 - 1) A_1 L G_2 + G_2 - 1), \tag{3.10}$$

$$P_{\mathrm{n,out,max}} = 2 n_{\mathrm{sp}} h\nu\Delta\nu((G_1 - 1) A_1 L A_2 G_2 + G_2 - 1), \tag{3.11}$$

$$\mathrm{OSNR}_{\mathrm{min}} = \frac{P_{\mathrm{s,min}}}{2 n_{\mathrm{sp}} h\nu\Delta\nu} \frac{G_1 A_1 L G_2}{(G_1 - 1) A_1 L G_2 + G_2 - 1}, \tag{3.12}$$

$$\approx \frac{P_{\mathrm{s,min}}}{2 n_{\mathrm{sp}} h\nu\Delta\nu} \frac{G_1 A_1 L}{G_1 A_1 L + 1} \tag{3.13}$$

$$\mathrm{OSNR}_{\mathrm{max}} = \frac{P_{\mathrm{s,min}}}{2 n_{\mathrm{sp}} h\nu\Delta\nu} \frac{G_1 A_1 L G_2}{(G_1 - 1) A_1 L A_2 G_2 + G_2 - 1}, \tag{3.14}$$

We can note, from equations 3.12 and 3.14, since $A_2 < 1$, the OSNR will always be lowest for the lowest powered input line. Since the pulse shaper used in the flattening stage has a maximum allowed input power per line, we will have to take that into account. Assuming that it is fixed at P_{shaper}, we have to set the attenuation A_1 such that $P_{\mathrm{s,min}} F G_1 A_1 = P_{\mathrm{shaper}}$. The requirements for the minimum power will then be:

$$P_{\mathrm{s,min}} = \mathrm{OSNR}_{\mathrm{req}} 2 n_{\mathrm{sp}} h\nu\Delta\nu \frac{1}{1 - F \frac{\mathrm{OSNR}_{\mathrm{req}} 2 n_{\mathrm{sp}} h\nu\Delta\nu}{L P_{\mathrm{shaper}}}}. \tag{3.15}$$

For the same EDFA values as before, using a pulse shaper with $P_{\mathrm{shaper}} = 13\,\mathrm{dBm}$ and $L = 1/4\,(-6\,\mathrm{dB})$ and a comb with 20 dB flatness we require $P_{\mathrm{s,min}} \approx -16.3\,\mathrm{dBm}$. For a 16QAM link, using identical parameters, the required minimum power per line would instead be $-23.6\,\mathrm{dBm}$. Changing the comb flatness will give slightly different numbers, figure 3.3 illustrates this.

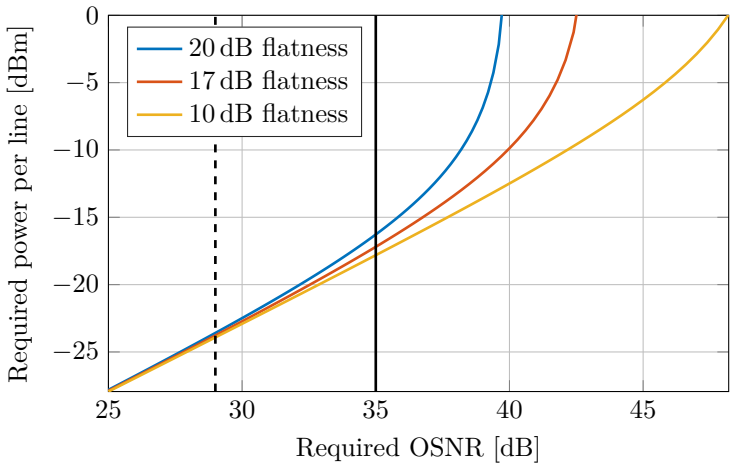

Figure 3.3. The required minimum power per line as a function of required OSNR for combs of different flatness according to equation 3.15. The EDFA and flattening stage parameters are as follows: $2n_{\mathrm{sp}} = 5\,\mathrm{dB}$, $\nu = c/1550\,\mathrm{nm}$, $\Delta\nu = 12.5\,\mathrm{GHz}$, $L = -6\,\mathrm{dB}$ and $P_{\mathrm{shaper}} = 13\,\mathrm{dBm}$. The solid line indicates the required OSNR for a single-span 64QAM link, while the dashed line shows the requirements for an identical link using 16QAM.

Chapter 4

Microresonator physics

This chapter describes the basic operating principle of microresonator frequency combs. The linear operation will be described first, with a more complete model, including the important nonlinear effects, being presented in the later part of the chapter.

4.1 The linear regime

In the most basic picture, a microresonator can be described as a loop system with one, or in the case of a drop port being present, two couplers. Figure 4.1 shows a basic sketch, noting the complex electric fields at certain positions.

The coupling of the fields between the different paths can be described

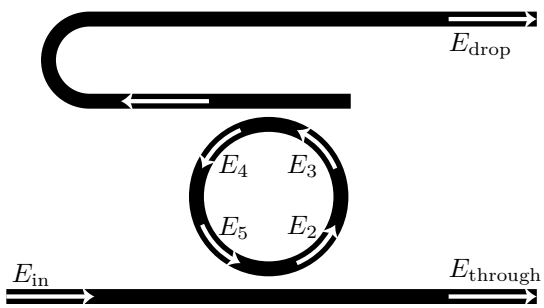

Figure 4.1. A sketch of a simple ring resonator system.

using the following equations [76, 77]:

$$\begin{bmatrix} E_{\text{through}} \\ E_2 \end{bmatrix} = \begin{bmatrix} t & \kappa \\ -\kappa^* & t^* \end{bmatrix} \begin{bmatrix} E_{\text{in}} \\ E_5 \end{bmatrix}, \tag{4.1}$$

$$\begin{bmatrix} E_{\text{drop}} \\ E_4 \end{bmatrix} = \begin{bmatrix} t_{\text{d}} & \kappa_{\text{d}} \\ -\kappa_{\text{d}}^* & t_{\text{d}}^* \end{bmatrix} \begin{bmatrix} 0 \\ E_3 \end{bmatrix}, \tag{4.2}$$

$$E_3 = \exp\left(-\frac{\alpha}{2}\frac{L}{2}\right) \exp\left(i\beta\frac{L}{2}\right) E_2, \tag{4.3}$$

$$E_5 = \exp\left(-\frac{\alpha}{2}\frac{L}{2}\right) \exp\left(i\beta\frac{L}{2}\right) E_4. \tag{4.4}$$

The two coupling regions are defined by the constants t, κ, t_{d}, and κ_{d}, such that $|t|^2 + |\kappa|^2 = 1$ and $|t_{\text{d}}|^2 + |\kappa_{\text{d}}|^2 = 1$. The waveguide in the ring is assumed to have a power propagation loss per length of $-\alpha$ and a propagation constant β while L corresponds to the length of the resonator. The power out at the through and drop port can then directly be derived:

$$|E_{\text{through}}|^2 = |E_{\text{in}}|^2 \times \frac{|t|^2 + |t_{\text{d}}|^2 \exp(-L\alpha) - 2\exp\left(-\frac{\alpha}{2}L\right)|t||t_{\text{d}}|\cos(\beta L - \phi_t - \phi_{t,\text{d}})}{1 + |t|^2|t_{\text{d}}|^2\exp(-L\alpha) - 2\exp\left(-\frac{\alpha}{2}L\right)|t||t_{\text{d}}|\cos(\beta L - \phi_t - \phi_{t,\text{d}})}, \tag{4.5}$$

$$|E_{\text{drop}}|^2 = |E_{\text{in}}|^2 \times \frac{\exp\left(-\frac{\alpha}{2}L\right)|\kappa|^2|\kappa_{\text{d}}|^2}{1 + |t|^2|t_{\text{d}}|^2\exp(-L\alpha) - 2\exp\left(-\frac{\alpha}{2}L\right)|t||t_{\text{d}}|\cos(\beta L - \phi_t - \phi_{t,\text{d}})}. \tag{4.6}$$

For clearer visibility, the transmission coefficients have been expanded according to $t = |t|\exp(i\phi_t)$ and $t_{\text{d}} = |t_{\text{d}}|\exp(i\phi_{t,\text{d}})$. The case where there is no drop port can be trivially extracted by setting $t_{\text{d}} = 1$ and $\kappa_{\text{d}} = 0$.

When pumping at a resonance, that is when $\beta L - \phi_t - \phi_{t,\text{d}} = 2\pi m$, with m being an integer, the power present at the through port is minimized. One potentially interesting special case in that situation is that of critical coupling, this occurs when the coupling losses at the input are equal to the rest of the losses in the cavity:

$$|t| = \exp\left(-\frac{\alpha}{2}L\right)|t_d|. \tag{4.7}$$

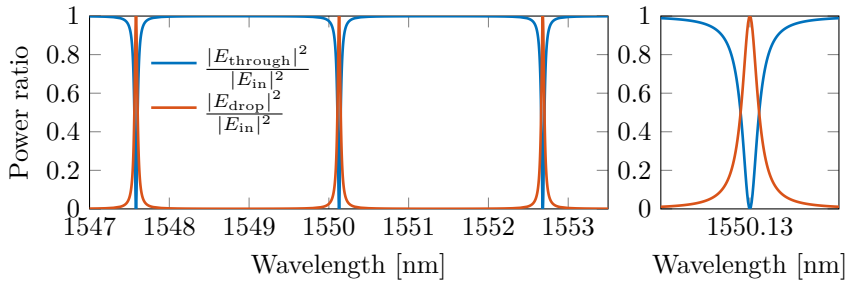

Figure 4.2. (Left) Example scan for a critically coupled ring with the following parameters: $\alpha = 0$, $L = 2\pi 100\,\mu\text{m}$, $|t|^2 = |t_\text{d}|^2 = 0.95$, $\phi_t = \phi_{t,\text{d}} = 0$, $\beta = n_\text{eff}\frac{2\pi}{\lambda}$, $n_\text{eff} = 1.5$. (Right) Zoomed-in view of one of the coupling regions showing the symmetry between the two ports.

In this situation, at resonance, equations 4.5 and 4.6 become:

$$|E_\text{through}|^2 = 0, \tag{4.8}$$

$$|E_\text{drop}|^2 = |E_\text{in}|^2 \frac{\frac{|t|}{|t_\text{d}|} - |t||t_\text{d}|}{1 - |t|^2}. \tag{4.9}$$

In the case where there is no drop port (i.e. $|t_\text{d}| = 1$), equation 4.8 shows that the losses in the ring absorb the full power from the pump leaving nothing at the through port. On the other hand if there is a drop port, we can see from equation 4.7 that if we want to keep the critical coupling we have to decrease the losses, α, at the same time as increasing the coupling strength of the drop port. In the special case of $|t_\text{d}| = |t|$, the losses have to become zero! In this case the output power at the drop port, according to equation 4.9 will be equal to the input: $|E_\text{drop}|^2 \xrightarrow{t_\text{d}\to t} |E_\text{in}|^2$. Here, it is important to note that these equations are valid in the linear propagation regime. When the Kerr effect is included and the power in the resonator is sufficiently high, the pump depletion will cause additional losses for the pump wave. This will lead to the coupling not being effectively critical anymore. It has been shown that it is possible to compensate for this by increasing the coupling strength, making the system overcoupled in the linear regime [78].

4.1.1 The coupling region

Above, the coupling between the bus waveguide and the ring itself was characterized with a single constant κ. This parameter is naturally dependent on

a couple of things, specifically the interaction length and the mode overlap between the modes of the two waveguides [79]. For well confined modes for instance, the mode overlap will be low, leading to a weak coupling unless the interaction length is extended accordingly. It is also important to note that modes of different polarizations will couple to a different extent, enabling the design of components for polarization splitting [80]. The easiest way to increase the coupling interaction length is to make the bus waveguide follow the resonator over a part of a round-trip in a "pulley" coupling scheme [81]. This results in an extra tunable degree of freedom for the coupling constant.

4.1.2 Characterizing the linear parameters

By sweeping the wavelength of a continuous-wave (CW) pump laser, we can observe and extract information about the ring. Figure 4.2 demonstrates the wavelength dependence of both outputs in the lossless, critically coupled case, assuming that the waveguide has no dispersion. Next, we will derive a model for extracting useful parameters in the presence of both-nonlinear coupling and a non-zero dispersion from such a scan. The easiest thing to measure in practice is the full width at half maximum (FWHM) of a resonance. In the general case, where the coupling might not be critical, the half maximum is defined as the point where the throughput power is exactly half-way between the minimum and the maximum. This can be related to the losses of the ring by extracting the $\Delta\beta_{\mathrm{FWHM}}$ from equation 4.5:

$$\Delta\beta_{\mathrm{FWHM}}L = 2\cos^{-1}\left(\frac{1+|t|^2|t_{\mathrm{d}}|^2\exp(-\alpha L)}{2-2|t||t_{\mathrm{d}}|\exp\left(-\frac{\alpha}{2}L\right)+2|t|^2|t_{\mathrm{d}}|^2\exp(-\alpha L)}\right) \tag{4.10}$$

$$\approx 2\left(1-|t||t_{\mathrm{d}}|\exp\left(-\frac{\alpha}{2}L\right)\right). \tag{4.11}$$

By Tailor-expanding around the one-sided limit of $|t||t_{\mathrm{d}}|\exp\left(-\frac{\alpha}{2}L\right)\to 1^-$, we arrive at the formula above. Assuming that the group index, n_{g}, is constant across one resonance, we can relate this to measurements by approximating $\Delta\beta$:

$$|\Delta\beta| \approx \frac{2\pi n_{\mathrm{g}}|\Delta\lambda|}{\lambda^2}. \tag{4.12}$$

This will result in the following relation between the FWHM and the losses:

$$\Delta\lambda_{\mathrm{FWHM}} \approx \frac{\lambda^2}{\pi n_{\mathrm{g}}L}\left(1-|t||t_{\mathrm{d}}|\exp\left(-\frac{\alpha}{2}L\right)\right). \tag{4.13}$$

However, to accurately convert between the resonance FWHM and the loss parameters, we need to know the group index, n_g, of the material. Fortunately, we can figure that one out by finding the wavelengths for two adjacent resonances and calculating the free spectral range (FSR). We know, by assuming that the couplers' phase shifts ϕ_t and $\phi_{t,d}$ are constant between the adjacent resonances, that $|\beta(\lambda_1)L - \beta(\lambda_2)L| = 2\pi$. By also assuming that the group index is identical for adjacent resonances (this assumption might not be valid for rings with strong dispersion and large FSR!), we can extract:

$$\Delta\lambda_{\mathrm{FSR}} \approx \frac{\lambda^2}{n_g L}. \tag{4.14}$$

To disentangle the different loss contributions one can also look at the extinction ratio for the through port:

$$\frac{|E_{\mathrm{through,max}}|^2}{|E_{\mathrm{through,min}}|^2} = \frac{\left(1 - |t||t_d| \exp\left(-\frac{\alpha}{2}L\right)\right)^2 \left(|t|^2 + |t_d|^2 \exp\left(-\alpha L\right)\right)}{\left(|t_d| \exp\left(-\frac{\alpha}{2}L\right) - |t|\right)^2 \left(1 + |t|^2|t_d|^2 \exp\left(-\alpha L\right)\right)}. \tag{4.15}$$

By measuring $\Delta\lambda_{\mathrm{FWHM}}$ and the extinction ratio we can then, using equations 4.13 and 4.15, numerically extract the two parameters: $|t|$ and $|t_d| \exp\left(-\frac{\alpha}{2}L\right)$. In the case of a symmetrically coupled resonator with very weak coupling (i.e. where $|t| = |t_d| \approx 1$) this can be simplified further [82]:

$$\frac{|E_{\mathrm{through,max}}|^2}{|E_{\mathrm{through,min}}|^2} \approx \frac{\left(\Delta\lambda_{\mathrm{FWHM}} \frac{\pi n_g L}{\lambda^2}\right)^2}{\left(1 - \exp\left(-\frac{\alpha}{2}L\right)\right)^2} \approx \frac{\left(\pi \frac{\Delta\lambda_{\mathrm{FWHM}}}{\Delta\lambda_{\mathrm{FSR}}}\right)^2}{\left(1 - \exp\left(-\frac{\alpha}{2}L\right)\right)^2}. \tag{4.16}$$

4.2 Light propagation and the Kerr effect

To understand the way the light and the ring resonators interact, we will have to look at the nonlinear Kerr effect. Light-matter interaction in general is described by Maxwell's equations. Their full analysis is beyond the scope of this thesis but can be found in reference [83]. They predict that for high optical intensities, such as the ones we will encounter inside the rings, the material will allow for nonlinear interactions between photons of different wavelengths. The part that concerns us the most is the interaction facilitated by the third-order susceptibility, $\chi^{(3)}$, causing the refractive index of the mode in the material to be intensity-dependent [83]:

$$n(\lambda, I) = n_0(\lambda) + n_2(\lambda) I. \tag{4.17}$$

To analyze waves propagating through a fiber or a waveguide, it is typically enough to model the field envelopes, A, rather than the electric field itself, where the amplitude is normalized such that $|A|^2 = I$. With this assumption, one can derive the nonlinear Schrödinger equation (NLSE) for the propagating waves [83]:

$$\frac{\partial A}{\partial z} = -\frac{\alpha}{2}A + i\sum_{k\geq 2}\frac{\beta_k}{k!}\left(i\frac{\partial}{\partial t}\right)^k A + i\gamma|A|^2 A. \tag{4.18}$$

Here, α denotes the fiber power losses per unit length while β_k denotes the k-th coefficient in the Taylor expansion of the frequency-dependent propagation constant of the material. The nonlinear parameter, γ, is related to the intensity-dependent refractive index, n_2, and the effective mode area, A_{eff}:

$$\gamma = \frac{\omega n_2}{cA_{\text{eff}}}. \tag{4.19}$$

For materials with high confinement and modes that are not fully transverse electromagnetic, the effective area in each material region, A_{NL}, requires full vectorial knowledge of the mode. It can then be calculated using [84]:

$$A_{\text{eff}} = \frac{\mu_0}{\epsilon_0 n_0^2}\frac{\left[\int_{A_\infty}(\boldsymbol{e}_\text{t}\times\boldsymbol{h}_\text{t})\cdot\hat{\boldsymbol{z}}\,\text{d}x\text{d}y\right]^2}{\int_{A_{\text{NL}}}\left[(\boldsymbol{e}_\text{t}\cdot\boldsymbol{e}_\text{t})^2 + 2/3|e_\text{z}|^2\boldsymbol{e}_\text{t}\cdot\boldsymbol{e}_\text{t} + |e_\text{z}|^4\right]\text{d}x\text{d}y}, \tag{4.20}$$

where $\boldsymbol{e}_\text{t}$ and $\boldsymbol{h}_\text{t}$ are the transverse components of the mode's electric and magnetic field respectively, while e_z is the electric field's longitudinal component. In a structure consisting of several different materials, the total effective nonlinear coefficient, γ, will then become:

$$\gamma = \frac{\omega\epsilon_0}{c\mu_0}\frac{\int_{A_\infty} n_0(x,y)^2 n_2(x,y)\left[(\boldsymbol{e}_\text{t}\cdot\boldsymbol{e}_\text{t})^2 + 2/3|e_\text{z}|^2\boldsymbol{e}_\text{t}\cdot\boldsymbol{e}_\text{t} + |e_\text{z}|^4\right]\text{d}x\text{d}y}{\left[\int_{A_\infty}(\boldsymbol{e}_\text{t}\times\boldsymbol{h}_\text{t})\cdot\hat{\boldsymbol{z}}\,\text{d}x\text{d}y\right]^2}. \tag{4.21}$$

4.3 The Lugiato-Lefever equation

To get a more complete picture of what happens in a ring geometry, including the Kerr effect, one would like to combine equations 4.1, 4.2 and 4.18. While numerical simulations can be done in a straightforward way on these directly, they do not help in qualitative understanding. To get a single closed form

expression that we can derive understanding from, we will have to make some additional assumptions and simplifications.

In this section we will be dealing with resonator devices without a drop port and with the assumption that the coupling between two waveguides adds a π phase shift while the transmission over one coupling region does not change the phase: $\kappa = -\sqrt{\theta}$ and $t = \sqrt{1-\theta}$. We will also assume that the wave envelope barely changes over one roundtrip: $A(L,t) \approx A(0,t) + L\frac{\partial A}{\partial z}$. Since we're working with the field envelope in the NLSE, the phase evolution over one roundtrip will not be present, we will however still need to take into account a relative phase offset, ϕ:

$$A_2 = \sqrt{\theta}A_{\text{in}} + \sqrt{1-\theta}\exp(i\phi)A_5, \tag{4.22}$$

$$A_5 = A_2 + L\frac{\partial A}{\partial z}. \tag{4.23}$$

The phase offset, ϕ, corresponds to the relative phase drift of the wave compared to the phase of a wave at a resonance wavelength: $\phi = \Delta\beta L \approx \Delta\nu\frac{2\pi L n_g}{c}$ and is applied at the end of each roundtrip. Assuming that we have a weakly coupled resonator pumped close to a resonance, both θ and ϕ are small. We can then Taylor expand them according to:

$$\sqrt{1-\theta} \approx 1 - \frac{\theta}{2}, \tag{4.24}$$

$$\exp(i\phi) \approx 1 + i\phi. \tag{4.25}$$

Inserting this back into equation 4.22 and linearizing in terms of the variables θ, ϕ, and $\frac{\partial A}{\partial z}$ gives us an expression for the wave after roundtrip m:

$$A_2^{(m)} \approx \sqrt{\theta}A_{\text{in}} + A_2^{(m-1)}\left(1 - \frac{\theta}{2} + i\phi\right) + L\frac{\partial A}{\partial z}. \tag{4.26}$$

We can now insert equation 4.18. Since we know that the change between consecutive roundtrips is small, we can write a differential equation describing the slow time-evolution of the wave at this point assuming a roundtrip time of t_{r} [85, 86]:

$$\frac{\partial A}{\partial \tau} \approx \frac{A^{(m)} - A^{(m-1)}}{t_{\text{r}}} \tag{4.27}$$

$$= \frac{1}{t_{\text{r}}}\left[\left(-\frac{L\alpha+\theta}{2} + i\phi + iL\sum_{k\geq 2}\frac{\beta_k}{k!}\left(i\frac{\partial}{\partial t}\right)^k + i\gamma L|A|^2\right)A + \sqrt{\theta}A_{\text{in}}\right]. \tag{4.28}$$

This equation is generally known as the Lugiato-Lefever equation or the driven-and-damped nonlinear Schrödinger equation. It can be used to model microresonator systems, operating both in the linear and the nonlinear regime, as long as the pump detuning is not too large and the coupling strength is not too strong (i.e. while equations 4.24 and 4.25 are valid).

4.4 Comb initialization

Using the Lugiato-Lefever model in equation 4.28, it is then possible to predict the behavior of microresonator combs. A perturbation analysis around the CW steady-state gives useful information about the comb initialization process when pumping with a single CW pump [87–90]. The CW steady-state, A_s, can be found by setting all time derivatives in equation 4.28 to zero:

$$0 = \left(-\frac{L\alpha+\theta}{2} + i\phi + i\gamma L|A_\mathrm{s}|^2\right)A_\mathrm{s} + \sqrt{\theta}A_\mathrm{in} \Rightarrow \tag{4.29}$$

$$\theta|A_\mathrm{in}|^2 = |A_\mathrm{s}|^2\left(\left(\frac{L\alpha+\theta}{2}\right)^2 + \phi^2\right) + |A_\mathrm{s}|^4 2\phi\gamma L + |A_\mathrm{s}|^6\gamma^2L^2. \tag{4.30}$$

Depending on the pumping region, this equation has between one and three solutions for $|A_\mathrm{s}|^2$. The solution(s) can be found numerically if one knows all the initial parameters. Starting from such a steady-state position, by applying a small perturbation, A_p, equation 4.28 gives:

$$A = A_\mathrm{s} + A_\mathrm{p}, \tag{4.31}$$

$$\begin{aligned} t_\mathrm{r}\frac{\partial A_\mathrm{p}}{\partial\tau} = &\left(-\frac{L\alpha+\theta}{2} + i\phi + iL\sum_{k\geq 2}\frac{\beta_k}{k!}\left(i\frac{\partial}{\partial t}\right)^k\right)A_\mathrm{p} + \\ &+ i\gamma L(A_\mathrm{s}^2A_\mathrm{p}^* + 2|A_\mathrm{s}|^2A_\mathrm{p} + 2A_\mathrm{s}|A_\mathrm{p}|^2 + A_\mathrm{s}^*A_\mathrm{p}^2 + A_\mathrm{p}^2A_\mathrm{p}^*). \end{aligned} \tag{4.32}$$

Assuming that the perturbation is small, $|A_\mathrm{p}| \ll |A_\mathrm{s}|$, equation 4.32 can be simplified to:

$$t_\mathrm{r}\frac{\partial A_\mathrm{p}}{\partial\tau} = \left(-\frac{L\alpha+\theta}{2} + i\phi + iL\sum_{k\geq 2}\frac{\beta_k}{k!}\left(i\frac{\partial}{\partial t}\right)^k + 2i\gamma LP_0\right)A_\mathrm{p} + i\gamma LA_\mathrm{s}^2A_\mathrm{p}^*, \tag{4.33}$$

where $P_0 = |A_\mathrm{s}|^2$. This is now a linear differential equation in $A_\mathrm{p}(t,\tau)$. To find the solutions with gain, one can set the following ansatz:

$$A_\mathrm{p}(t,\tau) = A_{-1}(\tau)\exp(-i\Delta\omega t) + E_1(\tau)\exp(i\Delta\omega t). \tag{4.34}$$

Plugging this back into equation 4.33 and separating the two frequency components, $\exp(-i\Delta\omega t)$ and $\exp(i\Delta\omega t)$, gives the following two coupled differential equations:

$$t_\mathrm{r}\frac{\partial A_{-1}}{\partial \tau} = \left(-\frac{L\alpha+\theta}{2} + i\phi + 2i\gamma L P_0 + iL\sum_{k\geq 2}\frac{\beta_k}{k!}i^k(-i\Delta\omega)^k\right)A_{-1} + i\gamma L A_\mathrm{s}^2 A_1^* \tag{4.35}$$

$$t_\mathrm{r}\frac{\partial A_{1}}{\partial \tau} = \left(-\frac{L\alpha+\theta}{2} + i\phi + 2i\gamma L P_0 + iL\sum_{k\geq 2}\frac{\beta_k}{k!}i^k(i\Delta\omega)^k\right)A_{1} + i\gamma L A_\mathrm{s}^2 A_{-1}^*. \tag{4.36}$$

The solutions to these differential equations are:

$$t_\mathrm{r}A_{-1}(\tau) = C_1\exp(m_1\tau) + C_2\exp(m_2\tau), \tag{4.37}$$

$$t_\mathrm{r}A_{1}(\tau) = C_3\exp(m_1^*\tau) + C_4\exp(m_2^*\tau), \tag{4.38}$$

with

$$m_1 = -\frac{L\alpha+\theta}{2t_\mathrm{r}} + \frac{iL}{t_\mathrm{r}}\sum_{k\geq 3,\mathrm{odd}}\frac{\beta_k}{k!}\Delta\omega^k - \frac{1}{t_\mathrm{r}}\sqrt{\gamma^2L^2P_0^2 - \left(\phi + 2\gamma LP_0 + L\sum_{k\geq 2,\mathrm{even}}\frac{\beta_k}{k!}\Delta\omega^k\right)^2}, \tag{4.39}$$

$$m_2 = -\frac{L\alpha+\theta}{2t_\mathrm{r}} + \frac{iL}{t_\mathrm{r}}\sum_{k\geq 3,\mathrm{odd}}\frac{\beta_k}{k!}\Delta\omega^k + \frac{1}{t_\mathrm{r}}\sqrt{\gamma^2L^2P_0^2 - \left(\phi + 2\gamma LP_0 + L\sum_{k\geq 2,\mathrm{even}}\frac{\beta_k}{k!}\Delta\omega^k\right)^2}. \tag{4.40}$$

The effective frequency-dependent gain will then correspond to the real part of m_2. Important to note is that for there to be net gain, the term under the square root has to remain positive and be large enough to compensate

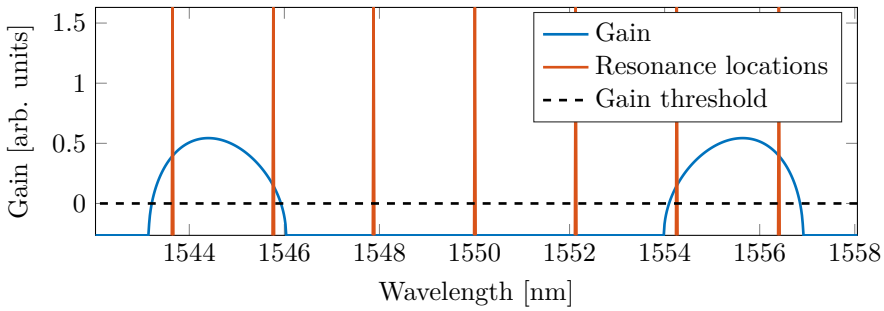

Figure 4.3. An example initial gain spectrum for a ring with the resonance locations plotted on top.

for both the propagation losses and the coupling losses. Figure 4.3 shows an example gain spectrum. For the gain to be maximized at a certain frequency offset, $\Delta\omega$, there will therefore be requirements on the physical parameters:

$$\phi + 2\gamma L P_0 + L \sum_{k\geq 2,\text{even}} \frac{\beta_k}{k!}\Delta\omega^k = 0. \tag{4.41}$$

This means that a negative β_2 is optimum for maximum peak gain or in the case of a slightly positive β_2, a red-shift of the pump compared to the resonance, setting $\phi < 0$ can also work. In practice, a red-detuned pump is difficult to stabilize with respect to the cavity wavelength because of thermal effects that will be described sin section 4.6.1.

4.4.1 Soliton generation

When operating in the anomalous dispersion regime, where $\beta_2 < 0$, assuming low losses, one solution to the Lugiato-Lefever equation is a train of solitons. These are pulse forms where the Kerr nonlinearity of the resonator medium has counteracted the anomalous dispersion in terms of phase shift. They can typically be generated by careful tuning of the CW pump into the resonance. The dynamics are somewhat chaotic however as the final state and the tuning path depends on the initial noise state [90–93]. To achieve full deterministic control over the number of solitons in the cavity as well as long term stability, more feedback and laser [94–97] or thermal [98] tuning is required. Since devices that are thick enough to have anomalous dispersion are also multi-mode, there is a risk for mode interaction happening when attempting to generate very wide

combs. These higher-order modes can however be suppressed using filtering sections [99].

4.4.2 The normal dispersion regime

The Lugiato-Lefever model predicts that for simple CW pumps, the resonators need anomalous dispersion around the pumping region if one wishes to avoid red-detuning the pump with respect to the resonance. This criterion can be sidestepped in a few ways enabling combs using waveguides with normal dispersion. Pumping the resonators with multiple pumps, or a single RF-modulated pump can provide the first frequency components from which the rest can grow through four-wave mixing (FWM) [100–102]. This multi-pump situation can be modelled using the Lugiato-Lefever equation as well [103] leading to solutions that qualitatively agree with experiments. This situation is discussed in [Paper B].

Another way to counteract the normal dispersion is to design the waveguide so that, around the pump location, the dispersion becomes locally anomalous. In multi-mode waveguides the geometry can be designed so that higher order modes couple to the pumped mode at some wavelength leading to a locally strong anomalous dispersion [55, 104–107]. Figure 4.4 shows how this would look like for two coupled modes. The resonator used in [Paper A] is enabled using such an interaction. In these circumstances the comb is initialized using the degenerate FWM process that was described above, while the new lines are then grown using non-degenerate FWM. The pump laser wavelength requires fine-tuning here as well since there are several different operating modes with different noise properties [108].

Another way to locally perturb a mode is by coupling it with its own counterpropagating version with the help of periodic perturbations in the waveguide [109] or using additional structures to alter the mode of interest [110–112]. All these methods require careful design and in some cases possibility for additional microheater tuning afterwards.

4.5 Noise properties

At the output of microresonator frequency combs, it is possible to observe different kinds of noise. The most trivial kind is the one present around the lines originating from the initial noise in the pump. This is however not the only noise present at the output. Depending on the detuning of the pump with respect to the utilized resonance, one can observe both wide and narrow, beat

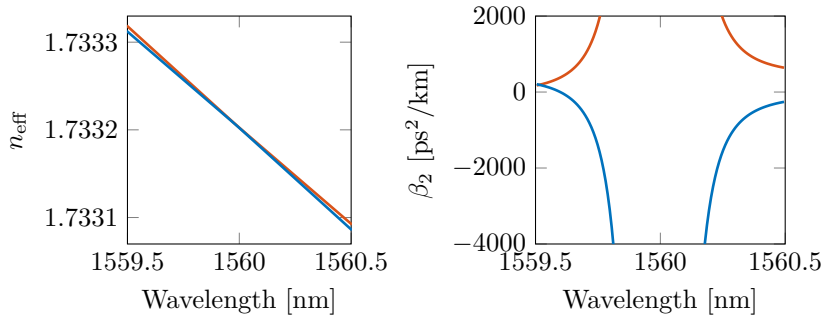

Figure 4.4. Simulated example where two modes interact. (Left) showing the effective index, n_{eff}, with the barely avoided crossing and (Right) showing the resulting perturbed dispersion, β_2 for the two modes.

note-like, intensity noise around the lines [55]. The beat note-like noise can be present due to two or more comb formations happening simultaneously with different spacings [53, 108]. Additional models exist predicting similar beat notes to appear due to perturbations such as higher order dispersion [113].

4.6 Other practical considerations

4.6.1 The temperature

A physical parameter that has gotten little mention in this thesis so far is the temperature. The refractive index of most materials is temperature dependent and since microresonators are typically pumped with high powered laser light, the temperature of chips under operation is expected to be higher than room temperature. When tuning a pump laser into a resonance, more and more power gets coupled into the ring, thus increasingly heating it up. This causes a red-shift of the resonance [114]. Since the resonances shift towards longer wavelengths regardless of the direction of the pump sweep, this leads to an asymmetric transmission scan that is different depending on the sweeping direction [115]. In practice, this also means that only a blue-detuned pump can be thermally stable. A small increase in the pump wavelength will cause the resonance location to shift away from the pump in the red-detuned case at which point the power level in the resonator decreases and causes the resonance to shift even further. See figure 4.5 for a sketch of this in action.

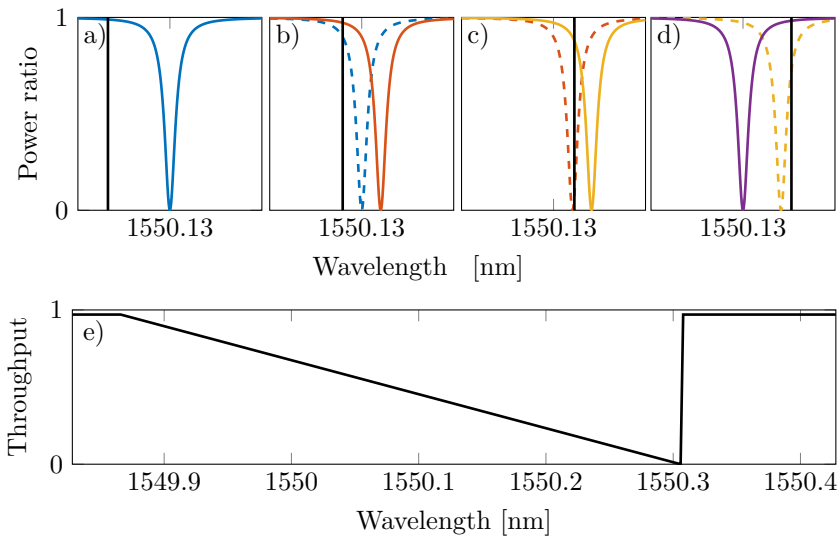

Figure 4.5. When the temperature of the chip changes, the resonance location is shifted. The plots show a sketch of the time evolution of a resonance when the laser is slowly tuned past it. The solid black line represents the pump laser, the solid colored curve is the resonance's current state, while the colored dashed curve is the resonance's previous state. a) The pump is blue-detuned from the resonance, the chip is cold. b) The laser approaches the resonance, thereby heating it up and causing it to red-shift. c) The laser continues approaching the resonance, heating it up even more. d) The laser has now passed the resonance, attempting to pump it in a red-detuned fashion, causing it to swiftly cool down and move back to its original location. The laser is therefore now far away from it. e) Plot showing the throughput as seen by a power meter while the laser is sweeping, note the asymmetrical shape of it showing the difficulty of pumping on the red side.

4.6.2 Conversion efficiency and the drop port

To relate this chapter back to the practical requirements for the communication applications, the conversion efficiency and flatness should be mentioned. The soliton and the normal dispersion combs behave very differently in this regard. In published experiments both system types operate in a configuration where a significant amount of the pump power is passed through giving an intrinsic flatness penalty that has to be taken care of by external filtering using a pulse shaper and/or a notch filter. A useful alternative to this penalty is implementing a drop port whose output better mirrors the intracavity comb state [116, 117].

For the normal dispersion combs conversion efficiencies (not counting fiber-to-chip coupling losses) above $-15\,\mathrm{dB}$ have been reported [116]. In some cases they have yielded several tens of lines far above the minimum power requirement from chapter 3 with the only potential weakness being the flatness [118].

In the soliton case much broader combs spanning two thirds of an octave have been reported [119]. These are however limited in terms of conversion efficiency leading to a much lower power per line. The soliton-based combs have been shown to have a maximum conversion efficiency that is inversely proportional to the number of lines [120].

Chapter 5

Future outlook

Reaching the final chapter of this thesis, let's have a look at the future outlook. In the context of optical communication, there are several avenues left to pursue. We have now demonstrated that combs can in principle work as drop-in replacements for free-running lasers. The first step towards making them fully competitive would be to ensure that they truly can cover the necessary bandwidth. Can one, through experiments together with modeling and simulations, improve and predict the flatness of combs generated in multi-pumped microresonators? By extending the mode solver and propagation simulation tools we have, as well as using the low-dispersion chips that we now have access to, we now have an opportunity to investigate the tradeoffs between flatness and number of initial pump lines. The first step could be to do more extensive simulations on the multi-mode coupling region to design a coupler that minimizes the amount of pump power that leaks out during the comb operation.

The other direction would be to develop the comb-specific advantages in a transmission setup (i.e. not just using them as drop-in replacements). This would entail demonstrating concepts such as joint phase- and polarization-tracking to demonstrate higher noise tolerance. While this would not necessarily increase the total propagation distance as much as the nonlinear pre-distortion, complimenting the two techniques should be a good way of maximizing the comb's advantages. This will of course require the receiver to be based on a frequency comb as well. To perform proof-of-concept demonstrations however, one might be satisfied with only looking at two or three lines at a time, meaning that the receiver comb could be something as simple as a laser followed by an electro-optic modulator.

Chapter 6

Summary of papers

Paper A

"Long-haul coherent transmission using a silicon nitride microresonator-based frequency comb as WDM source," *Conference on lasers and electro-optics (CLEO)*, San Jose, USA, paper SM4F.2, 2016.

In this paper we present the results from a coherent long-haul transmission experiment. We transmitted PM-QPSK-modulated data over more than 6000 km using a recirculating fiber loop. The light source consisted of seven lines generated using a low-noise microresonator-based frequency comb manufactured at Purdue University, USA. This is the first demonstration of long-haul data transmission using microresonator-based combs as light sources showing that the technology fits the requirements of long-haul data transmission.

My contribution: I performed the transmission measurements, implemented the DSP code, wrote the paper, and presented the results at CLEO in San Jose, USA.

Paper B

"Triply resonant coherent four-wave mixing in silicon nitride microresonators," *Optics Letters*, vol. 40, no. 17, pp. 4006-4009, 2015.

Here we measured the changes in four-wave mixing efficiency inside a triply-pumped normal dispersion microresonator while varying the relative phases of the pump waves. The three waves were generated using a tunable laser and electro-optic modulator and were set to wavelengths matching three adjacent resonances in the microresonator. The microresonator was manufactured in a multi-project wafer run by LioniX in the Netherlands. Additionally a simplified analytical model was developed that qualitatively matches the measurements while more complete numerical simulations were performed that also match quantitatively. Simulations using similar pump parameters but with an anomalous dispersion resonator were also performed. The results of experiments, simulations and analytical model all indicate that controlling the relative phases in the pump waves is of critical importance when maximizing the four-wave mixing efficiency.

My contribution: I performed the measurements, calculated the model, implemented the simulations, and wrote the paper.

References

[1] Internet Engineering Task Force. (1990). A standard for the transmission of IP datagrams on avian carriers, [Online]. Available: `https://tools.ietf.org/pdf/rfc1149.pdf` (visited on 2016-05-29).

[2] T. H. Maiman, "Stimulated optical radiation in ruby", *Nature*, vol. 187, no. 4736, pp. 493–494, 1960.

[3] K. C. Kao and G. A. Hockham, "Dielectric-fibre surface waveguides for optical frequencies", *Proceedings of the Institution of Electrical Engineers*, vol. 113, no. 7, pp. 1151–1158, 1966.

[4] R. J. Mears, L. Reekie, I. M. Jauncey, and D. N. Payne, "Low-noise erbium-doped fibre amplifier operating at 1.54µm", *Electronics Letters*, vol. 23, no. 19, pp. 1026–1028, 1987.

[5] L. E. Hargrove, R. L. Fork, and M. A. Pollack, "Locking of He-Ne laser modes induced by synchronous intracavity modulation", *Applied Physics Letters*, vol. 5, no. 1, pp. 4–5, 1964.

[6] J. N. Eckstein, A. I. Ferguson, and T. W. Hänsch, "High-resolution two-photon spectroscopy with picosecond light pulses", *Physical Review Letters*, vol. 40, no. 13, pp. 847–850, 1978.

[7] T. Udem, J. Reichert, R. Holzwarth, and T. W. Hänsch, "Absolute optical frequency measurement of the cesium d_1 line with a mode-locked laser", *Physical Review Letters*, vol. 82, no. 18, pp. 3568–3571, 1999.

[8] T. Udem, R. Holzwarth, and T. W. Hänsch, "Optical frequency metrology", *Nature*, vol. 416, no. 6877, pp. 233–237, 2002.

[9] S. T. Cundiff and J. Ye, "Colloquium: Femtosecond optical frequency combs", *Reviews of Modern Physics*, vol. 75, no. 1, pp. 325–342, 2003.

[10] S. A. Diddams, D. J. Jones, J. Ye, S. T. Cundiff, J. L. Hall, J. K. Ranka, R. S. Windeler, R. Holzwarth, T. Udem, and T. W. Hänsch, "Direct link between microwave and optical frequencies with a 300 THz femtosecond

laser comb", *Physical Review Letters*, vol. 84, no. 22, pp. 5102–5105, 2000.

[11] R. Holzwarth, T. Udem, T. W. Hänsch, J. C. Knight, W. J. Wadsworth, and P. S. J. Russell, "Optical frequency synthesizer for precision spectroscopy", *Physical Review Letters*, vol. 85, no. 11, pp. 2264–2267, 2000.

[12] D. J. Jones, S. A. Diddams, J. K. Ranka, A. Stentz, R. S. Windeler, J. L. Hall, and S. T. Cundiff, "Carrier-envelope phase control of femtosecond mode-locked lasers and direct optical frequency synthesis", *Science*, vol. 288, no. 5466, pp. 635–639, 2000.

[13] S. A. Diddams, L. Hollberg, and V. Mbele, "Molecular fingerprinting with the resolved modes of a femtosecond laser frequency comb", *Nature*, vol. 445, no. 7128, pp. 627–630, 2007.

[14] T. Ideguchi, S. Holzner, B. Bernhardt, G. Guelachvili, N. Picqué, and T. W. Hänsch, "Coherent Raman spectro-imaging with laser frequency combs", *Nature*, vol. 502, no. 7471, pp. 355–358, 2013.

[15] A. Foltynowicz, T. Ban, P. Masłowski, F. Adler, and J. Ye, "Quantum-noise-limited optical frequency comb spectroscopy", *Physical Review Letters*, vol. 107, no. 23, p. 233 002, 2011.

[16] A. L. Wolf, J. Morgenweg, J. C. J. Koelemeij, S. A. van den Berg, W. Ubachs, and K. S. E. Eikema, "Direct frequency-comb spectroscopy of a dipole-forbidden clock transition in trapped $^{40}Ca^{+}$ ions", *Optics Letters*, vol. 36, no. 1, pp. 49–51, 2010.

[17] T. Steinmetz, T. Wilken, C. Araujo-Hauck, R. Holzwarth, T. W. Hänsch, L. Pasquini, A. Manescau, S. D'Odorico, M. T. Murphy, T. Kentischer, W. Schmidt, and T. Udem, "Laser frequency combs for astronomical observations", *Science*, vol. 321, no. 5894, pp. 1335–1337, 2008.

[18] X. Yi, K. Vahala, J. Li, S. Diddams, G. Ycas, P. Plavchan, S. Leifer, J. Sandhu, G. Vasisht, P. Chen, P. Gao, J. Gagne, E. Furlan, M. Bottom, E. C. Martin, M. P. Fitzgerald, G. Doppmann, and C. Beichman, "Demonstration of a near-IR line-referenced electro-optical laser frequency comb for precision radial velocity measurements in astronomy", *Nature Communications*, vol. 7, p. 10 436, 2016.

[19] M. T. Hassan, T. T. Luu, A. Moulet, O. Raskazovskaya, P. Zhokhov, M. Garg, N. Karpowicz, A. M. Zheltikov, V. Pervak, F. Krausz, and E. Goulielmakis, "Optical attosecond pulses and tracking the nonlinear response of bound electrons", *Nature*, vol. 530, no. 7588, pp. 66–70, 2016.

[20] L. C. Sinclair, I. Coddington, W. C. Swann, G. B. Rieker, A. Hati, K. Iwakuni, and N. R. Newbury, "Operation of an optically coherent

frequency comb outside the metrology lab", *Optics Express*, vol. 22, no. 6, pp. 6996–7006, 2014.

[21] J. Lee, Y.-J. Kim, K. Lee, S. Lee, and S.-W. Kim, "Time-of-flight measurement with femtosecond light pulses", *Nature Photonics*, vol. 4, no. 10, pp. 716–720, 2010.

[22] N. Schuhler, Y. Salvadé, S. Lévêque, R. Dändliker, and R. Holzwarth, "Frequency-comb-referenced two-wavelength source for absolute distance measurement", *Optics Letters*, vol. 31, no. 21, pp. 3101–3103, 2006.

[23] I. Coddington, W. C. Swann, L. Nenadovic, and N. R. Newbury, "Rapid and precise absolute distance measurements at long range", *Nature Photonics*, vol. 3, no. 6, pp. 351–356, 2009.

[24] I. Coddington, W. Swann, and N. Newbury, "Coherent multiheterodyne spectroscopy using stabilized optical frequency combs", *Physical Review Letters*, vol. 100, no. 1, 2008.

[25] G. Millot, S. Pitois, M. Yan, T. Hovhannisyan, A. Bendahmane, T. W. Hänsch, and N. Picqué, "Frequency-agile dual-comb spectroscopy", *Nature Photonics*, vol. 10, no. 1, pp. 27–30, 2015.

[26] I. Coddington, N. Newbury, and W. Swann, "Dual-comb spectroscopy", *Optica*, vol. 3, no. 4, pp. 414–426, 2016.

[27] V. Durán, S. Tainta, and V. Torres-Company, "Ultrafast electrooptic dual-comb interferometry", *Optics Express*, vol. 23, no. 23, pp. 30 557–30 569, 2015.

[28] T. M. Fortier, M. S. Kirchner, F. Quinlan, J. Taylor, J. C. Bergquist, T. Rosenband, N. Lemke, A. Ludlow, Y. Jiang, C. W. Oates, and S. A. Diddams, "Generation of ultrastable microwaves via optical frequency division", *Nature Photonics*, vol. 5, no. 7, pp. 425–429, 2011.

[29] J. J. McFerran, E. N. Ivanov, A. Bartels, G. Wilpers, C. W. Oates, S. A. Diddams, and L. Hollberg, "Low-noise synthesis of microwave signals from an optical source", *Electronics Letters*, vol. 41, no. 11, pp. 650–651, 2005.

[30] W. Liang, D. Eliyahu, V. S. Ilchenko, A. A. Savchenkov, A. B. Matsko, D. Seidel, and L. Maleki, "High spectral purity Kerr frequency comb radio frequency photonic oscillator", *Nature Communications*, vol. 6, p. 7957, 2015.

[31] C.-B. Huang, Z. Jiang, D. E. Leaird, J. Caraquitena, and A. M. Weiner, "Spectral line-by-line shaping for optical and microwave arbitrary waveform generations", *Laser & Photonics Review*, vol. 2, no. 4, pp. 227–248, 2008.

[32] S. T. Cundiff and A. M. Weiner, "Optical arbitrary waveform generation", *Nature Photonics*, vol. 4, no. 11, pp. 760–766, 2010.

[33] C. Reimer, M. Kues, P. Roztocki, B. Wetzel, F. Grazioso, B. E. Little, S. T. Chu, T. Johnston, Y. Bromberg, L. Caspani, D. J. Moss, and R. Morandotti, "Generation of multiphoton entangled quantum states by means of integrated frequency combs", *Science*, vol. 351, no. 6278, pp. 1176–1180, 2016.

[34] N. R. Newbury, "Searching for applications with a fine-tooth comb", *Nature Photonics*, vol. 5, no. 4, pp. 186–188, 2011.

[35] L. C. Sinclair, J. D. Deschênes, L. Sonderhouse, W. C. Swann, I. H. Khader, E. Baumann, N. R. Newbury, and I. Coddington, "Invited article: A compact optically coherent fiber frequency comb", *Review of Scientific Instruments*, vol. 86, no. 8, p. 081 301, 2015.

[36] H. Murata, A. Morimoto, T. Kobayashi, and S. Yamamoto, "Optical pulse generation by electrooptic-modulation method and its application to integrated ultrashort pulse generators", *IEEE Journal of Selected Topics in Quantum Electronics*, vol. 6, no. 6, pp. 1325–1331, 2000.

[37] R. Wu, V. Torres-Company, D. E. Leaird, and A. M. Weiner, "Supercontinuum-based 10-GHz flat-topped optical frequency comb generation", *Optics Express*, vol. 21, no. 5, pp. 6045–6052, 2013.

[38] D. C. Cole, K. Beha, F. N. Baynes, P. Del'Haye, A. Rolland, T. M. Fortier, F. Quinlan, S. Diddams, and S. B. Papp, "Self-referencing a 10 GHz electro-optic comb", in *Conference on lasers and electro-optics (CLEO)*, 2015, STh4N.5.

[39] T. J. Kippenberg, R. Holzwarth, and S. A. Diddams, "Microresonator-based optical frequency combs", *Science*, vol. 332, no. 6029, pp. 555–559, 2011.

[40] P. Del'Haye, A. Schliesser, O. Arcizet, T. Wilken, R. Holzwarth, and T. J. Kippenberg, "Optical frequency comb generation from a monolithic microresonator", *Nature*, vol. 450, no. 7173, pp. 1214–1217, 2007.

[41] A. A. Savchenkov, A. B. Matsko, V. S. Ilchenko, I. Solomatine, D. Seidel, and L. Maleki, "Tunable optical frequency comb with a crystalline whispering gallery mode resonator", *Physical Review Letters*, vol. 101, no. 9, p. 093 902, 2008.

[42] I. S. Grudinin, N. Yu, and L. Maleki, "Generation of optical frequency combs with a CaF_2 resonator", *Optics Letters*, vol. 34, no. 7, pp. 878–880, 2009.

[43] W. Liang, A. A. Savchenkov, A. B. Matsko, V. S. Ilchenko, D. Seidel, and L. Maleki, "Generation of near-infrared frequency combs from a

MgF_2 whispering gallery mode resonator", *Optics Letters*, vol. 36, no. 12, pp. 2290–2292, 2011.

[44] B. J. M. Hausmann, I. Bulu, V. Venkataraman, P. Deotare, and M. Lončar, "Diamond nonlinear photonics", *Nature Photonics*, vol. 8, no. 5, pp. 369–374, 2014.

[45] J. Li, H. Lee, T. Chen, and K. J. Vahala, "Low-pump-power, low-phase-noise, and microwave to millimeter-wave repetition rate operation in microcombs", *Physical Review Letters*, vol. 109, no. 23, p. 233 901, 2012.

[46] L. Razzari, D. Duchesne, M. Ferrera, R. Morandotti, S. Chu, B. E. Little, and D. J. Moss, "CMOS-compatible integrated optical hyper-parametric oscillator", *Nature Photonics*, vol. 4, no. 1, pp. 41–45, 2009.

[47] A. G. Griffith, R. K. W. Lau, J. Cardenas, Y. Okawachi, A. Mohanty, R. Fain, Y. H. D. Lee, M. Yu, C. T. Phare, C. B. Poitras, A. L. Gaeta, and M. Lipson, "Silicon-chip mid-infrared frequency comb generation", *Nature Communications*, vol. 6, p. 6299, 2015.

[48] H. Jung, C. Xiong, K. Y. Fong, X. Zhang, and H. X. Tang, "Optical frequency comb generation from aluminum nitride microring resonator", *Optics Letters*, vol. 38, no. 15, p. 2810, 2013.

[49] J. S. Levy, A. Gondarenko, M. A. Foster, A. C. Turner-Foster, A. L. Gaeta, and M. Lipson, "CMOS-compatible multiple-wavelength oscillator for on-chip optical interconnects", *Nature Photonics*, vol. 4, no. 1, pp. 37–40, 2010.

[50] Y. Okawachi, K. Saha, J. S. Levy, Y. H. Wen, M. Lipson, and A. L. Gaeta, "Octave-spanning frequency comb generation in a silicon nitride chip", *Optics Letters*, vol. 36, no. 17, pp. 3398–3400, 2011.

[51] F. Ferdous, H. Miao, D. E. Leaird, K. Srinivasan, J. Wang, L. Chen, L. T. Varghese, and A. M. Weiner, "Spectral line-by-line pulse shaping of on-chip microresonator frequency combs", *Nature Photonics*, vol. 5, no. 12, pp. 770–776, 2011.

[52] T. Herr, V. Brasch, J. D. Jost, C. Y. Wang, N. M. Kondratiev, M. L. Gorodetsky, and T. J. Kippenberg, "Temporal solitons in optical microresonators", *Nature Photonics*, vol. 8, no. 2, pp. 145–152, 2014.

[53] T. Herr, K. Hartinger, J. Riemensberger, C. Y. Wang, E. Gavartin, R. Holzwarth, M. L. Gorodetsky, and T. J. Kippenberg, "Universal formation dynamics and noise of Kerr-frequency combs in microresonators", *Nature Photonics*, vol. 6, no. 7, pp. 480–487, 2012.

[54] T. Herr, V. Brasch, J. D. Jost, I. Mirgorodskiy, G. Lihachev, M. L. Gorodetsky, and T. J. Kippenberg, "Mode spectrum and temporal

soliton formation in optical microresonators", *Physical Review Letters*, vol. 113, no. 12, p. 123 901, 2014.

[55] X. Xue, Y. Xuan, Y. Liu, P.-H. Wang, S. Chen, J. Wang, D. E. Leaird, M. Qi, and A. M. Weiner, "Mode-locked dark pulse Kerr combs in normal-dispersion microresonators", *Nature Photonics*, vol. 9, no. 9, pp. 594–600, 2015.

[56] V. Ataie, E. Temprana, L. Liu, E. Myslivets, B. P.-P. Kuo, N. Alic, and S. Radic, "Ultrahigh count coherent WDM channels transmission using optical parametric comb-based frequency synthesizer", *Journal of Lightwave Technology*, vol. 33, no. 3, pp. 694–699, 2015.

[57] T. Ohara, H. Takara, T. Yamamoto, H. Masuda, T. Morioka, M. Abe, and H. Takahashi, "Over-1000-channel ultradense WDM transmission with supercontinuum multicarrier source", *Journal of Lightwave Technology*, vol. 24, no. 6, pp. 2311–2317, 2006.

[58] J. Pfeifle, V. Brasch, M. Lauermann, Y. Yu, D. Wegner, T. Herr, K. Hartinger, P. Schindler, J. Li, D. Hillerkuss, R. Schmogrow, C. Weimann, R. Holzwarth, W. Freude, J. Leuthold, T. J. Kippenberg, and C. Koos, "Coherent terabit communications with microresonator Kerr frequency combs", *Nature Photonics*, vol. 8, no. 5, pp. 375–380, 2014.

[59] J. Pfeifle, A. Kordts, P. Marin, M. Karpov, M. Pfeiffer, V. Brasch, R. Rosenberger, J. Kemal, S. Wolf, W. Freude, t. kippenberg tobias, and C. Koos, "Full C and L-band transmission at 20 Tbit/s using cavity-soliton Kerr frequency combs", in *CLEO Postdeadline papers*, 2015, JTh5C.8.

[60] B. J. Puttnam, R. S. Luis, W. Klaus, J. Sakaguchi, J. M. Delgado Mendinueta, Y. Awaji, N. Wada, Y. Tamura, T. Hayashi, M. Hirano, and J. Marciante, "2.15 Pb/s transmission using a 22 core homogeneous single-mode multi-core fiber and wideband optical comb", in *European Conference on Optical Communication (ECOC)*, 2015, PDP.3.1.

[61] E. Temprana, E. Myslivets, B. P. P. Kuo, L. Liu, V. Ataie, N. Alic, and S. Radic, "Overcoming Kerr-induced capacity limit in optical fiber transmission", *Science*, vol. 348, no. 6242, pp. 1445–1448, 2015.

[62] E. Temprana, E. Myslivets, L. Liu, V. Ataie, A. Wiberg, B. P. P. Kuo, N. Alic, and S. Radic, "Two-fold transmission reach enhancement enabled by transmitter-side digital backpropagation and optical frequency comb-derived information carriers", *Optics Express*, vol. 23, no. 16, pp. 20 774–20 783, 2015.

[63] R. Slavik, S. G. Farwell, M. J. Wale, and D. J. Richardson, "Compact optical comb generator using InP tunable laser and push-pull modula-

tor", *IEEE Photonics Technology Letters*, vol. 27, no. 2, pp. 217–220, 2015.

[64] V. Corral, R. Guzmán, C. Gordón, X. J. M. Leijtens, and G. Carpintero, "Optical frequency comb generator based on a monolithically integrated passive mode-locked ring laser with a Mach-Zehnder interferometer", *Optics Letters*, vol. 41, no. 9, pp. 1937–1940, 2016.

[65] P. Marin, J. Pfeifle, J. N. Kemal, S. Wolf, K. Vijayan, N. Chimot, A. Martinez, A. Ramdane, F. Lelarge, W. Freude, and C. Koos, "8.32 Tbit/s coherent transmission using a quantum-dash mode-locked laser diode", in *Conference on lasers and electro-optics (CLEO)*, 2016, STh1F.1.

[66] J. Summers, W. Williams, P. Evans, D. Gold, M. Lai, T. Vallaitis, A. James, D. Pavinski, P. Studenkov, M. Ziari, D. Welch, F. Kish, M. Missey, J. Sena, J. Ou-Yang, S. Corzine, and M. Fisher, "Monolithic InP-based coherent transmitter photonic integrated circuit with 2.25 Tbit/s capacity", *Electronics Letters*, vol. 50, no. 16, pp. 1150–1152, 2014.

[67] M. J. R. Heck, J. F. Bauters, M. L. Davenport, D. T. Spencer, and J. E. Bowers, "Ultra-low loss waveguide platform and its integration with silicon photonics", *Laser & Photonics Reviews*, vol. 8, no. 5, pp. 667–686, 2014.

[68] International Telecommunication Union. (2012). Spectral grids for WDM applications: DWDM frequency grid, recommendation ITU-T G.694.1, [Online]. Available: `http://www.itu.int/rec/T-REC-G.694.1-201202-I` (visited on 2016-05-29).

[69] E. Ip, A. P. T. Lau, D. J. F. Barros, and J. M. Kahn, "Coherent detection in optical fiber systems", *Optics Express*, vol. 16, no. 2, pp. 753–791, 2008.

[70] G. P. Agrawal, "Loss management", in *Fiber-optic Communication Systems*, 4th ed., John Wiley & Sons, Inc., 2011, ch. 7, pp. 295–344.

[71] T. Xu, G. Jacobsen, S. Popov, J. Li, A. T. Friberg, and Y. Zhang, "Analytical estimation of phase noise influence in coherent transmission system with digital dispersion equalization", *Optics Express*, vol. 19, no. 8, pp. 7756–7768, 2011.

[72] T. Pfau, S. Hoffmann, and R. Noé, "Hardware-efficient coherent digital receiver concept with feedforward carrier recovery for M-QAM constellations", *Journal of Lightwave Technology*, vol. 27, no. 8, pp. 989–999, 2009.

[73] N. Argyris, S. Dris, C. Spatharakis, and H. Avramopoulos, "High performance carrier phase recovery for coherent optical QAM", in *Optical Fiber Communication Conference (OFC)*, 2015, W1E.1.

[74] Finisar Corporation. (2015). Product guide - Waveshaper family of optical processors, [Online]. Available: `https://www.finisar.com/sites/default/files/downloads/waveshaper_family_of_programmable_optical_processors_12_page_brochure_2015_web.pdf` (visited on 2016-05-29).

[75] Santec Corporation. (2016). Programmable optical filters, [Online]. Available: `http://www.santec.com/jp/wp-content/uploads/WSS-1000-C-E-v1.01402.pdf` (visited on 2016-05-29).

[76] A. Yariv, "Universal relations for coupling of optical power between microresonators and dielectric waveguides", *Electronics Letters*, vol. 36, no. 4, pp. 321–322, 2000.

[77] W. Bogaerts, P. De Heyn, T. Van Vaerenbergh, K. De Vos, S. Kumar Selvaraja, T. Claes, P. Dumon, P. Bienstman, D. Van Thourhout, and R. Baets, "Silicon microring resonators", *Laser & Photonics Reviews*, vol. 6, no. 1, pp. 47–73, 2012.

[78] P.-H. Wang, Y. Xuan, X. Xue, Y. Liu, J. Wang, D. E. Leaird, M. Qi, and A. M. Weiner, "Frequency comb-enhanced coupling in silicon nitride microresonators", in *Conference on lasers and electro-optics (CLEO)*, 2015, FTh1D.4.

[79] W.-P. Huang, "Coupled-mode theory for optical waveguides: An overview", *Journal of the Optical Society of America A*, vol. 11, no. 3, pp. 963–983, 1994.

[80] D. Dai and J. E. Bowers, "Novel ultra-short and ultra-broadband polarization beam splitter based on a bent directional coupler", *Optics Express*, vol. 19, no. 19, pp. 18 614–18 620, 2011.

[81] M. K. Chin and S. T. Ho, "Design and modeling of waveguide-coupled single-mode microring resonators", *Journal of Lightwave Technology*, vol. 16, no. 8, pp. 1433–1446, 1998.

[82] S. Xiao, M. H. Khan, H. Shen, and M. Qi, "Modeling and measurement of losses in silicon-on-insulator resonators and bends", *Optics Express*, vol. 15, no. 17, pp. 10 553–10 561, 2007.

[83] G. P. Agrawal, "Pulse propagation in fibers", in *Nonlinear Fiber Optics*, 5th ed., Academic Press, 2013, ch. 2, pp. 27–56.

[84] V. P. Tzolov, M. Fontaine, N. Godbout, and S. Lacroix, "Nonlinear self-phase-modulation effects: A vectorial first-order perturbation approach", *Optics Letters*, vol. 20, no. 5, pp. 456–458, 1995.

[85] L. Lugiato and R. Lefever, “Spatial dissipative structures in passive optical systems”, *Physical Review Letters*, vol. 58, no. 21, pp. 2209–2211, 1987.

[86] S. Coen, H. G. Randle, T. Sylvestre, and M. Erkintalo, “Modeling of octave-spanning Kerr frequency combs using a generalized mean-field Lugiato–Lefever model”, *Optics Letters*, vol. 38, no. 1, pp. 37–39, 2013.

[87] M. Haelterman, S. Trillo, and S. Wabnitz, “Dissipative modulation instability in a nonlinear dispersive ring cavity”, *Optics Communications*, vol. 91, no. 5,6, pp. 401–407, 1992.

[88] ——, “Additive-modulation-instability ring laser in the normal dispersion regime of a fiber”, *Optics Letters*, vol. 17, no. 10, pp. 745–747, 1992.

[89] C. Godey, I. V. Balakireva, A. Coillet, and Y. K. Chembo, “Stability analysis of the spatiotemporal Lugiato-Lefever model for Kerr optical frequency combs in the anomalous and normal dispersion regimes”, *Physical Review A*, vol. 89, no. 6, p. 063 814, 2014.

[90] V. Torres-Company, D. Castelló-Lurbe, and E. Silvestre, “Comparative analysis of spectral coherence in microresonator frequency combs”, *Optics Express*, vol. 22, no. 4, pp. 4678–4691, 2014.

[91] M. R. E. Lamont, Y. Okawachi, and A. L. Gaeta, “Route to stabilized ultrabroadband microresonator-based frequency combs”, *Optics Letters*, vol. 38, no. 18, pp. 3478–3481, 2013.

[92] S. Coen and M. Erkintalo, “Universal scaling laws of Kerr frequency combs”, *Optics Letters*, vol. 38, no. 11, pp. 1790–1792, 2013.

[93] M. Erkintalo and S. Coen, “Coherence properties of Kerr frequency combs”, *Optics Letters*, vol. 39, no. 2, pp. 283–286, 2014.

[94] K. Saha, Y. Okawachi, B. Shim, J. S. Levy, R. Salem, A. R. Johnson, M. A. Foster, M. R. E. Lamont, M. Lipson, and A. L. Gaeta, “Modelocking and femtosecond pulse generation in chip-based frequency combs”, *Optics Express*, vol. 21, no. 1, pp. 1335–1343, 2013.

[95] J. A. Jaramillo-Villegas, X. Xue, P.-H. Wang, D. E. Leaird, and A. M. Weiner, “Deterministic single soliton generation and compression in microring resonators avoiding the chaotic region”, *Optics Express*, vol. 23, no. 8, pp. 9618–9626, 2015.

[96] X. Yi, Q.-F. Yang, K. Youl, and K. Vahala, “Active capture and stabilization of temporal solitons in microresonators”, *Optics Letters*, vol. 41, no. 9, pp. 2037–2040, 2016.

[97] M. Karpov, H. Guo, E. Lucas, A. Kordts, M. H. P. Pfeiffer, G. Lichachev, V. E. Lobanov, M. L. Gorodetsky, and T. J. Kippenberg, “Universal

dynamics and controlled switching of dissipative Kerr solitons in optical microresonators", *ArXiv e-prints*, p. 1601.05036, 2016.

[98] C. Joshi, J. K. Jang, K. Luke, X. Ji, S. A. Miller, A. Klenner, Y. Okawachi, M. Lipson, and A. L. Gaeta, "Thermally controlled comb generation and soliton modelocking in microresonators", *Optics Letters*, vol. 41, no. 11, pp. 2565–2568, 2016.

[99] A. Kordts, M. H. P. Pfeiffer, H. Guo, V. Brasch, and T. J. Kippenberg, "Higher order mode suppression in high-Q anomalous dispersion SiN microresonators for temporal dissipative Kerr soliton formation", *Optics Letters*, vol. 41, no. 3, pp. 452–455, 2016.

[100] S. B. Papp, P. Del'Haye, and S. A. Diddams, "Parametric seeding of a microresonator optical frequency comb", *Optics Express*, vol. 21, no. 15, pp. 17 615–17 624, 2013.

[101] V. E. Lobanov, G. Lihachev, T. J. Kippenberg, and M. L. Gorodetsky, "Frequency combs and platicons in optical microresonators with normal GVD", *Optics Express*, vol. 23, no. 6, pp. 7713–7721, 2015.

[102] D. Strekalov and N. Yu, "Generation of optical combs in a whispering gallery mode resonator from a bichromatic pump", *Physical Review A*, vol. 79, no. 4, p. 041 805, 2009.

[103] T. Hansson and S. Wabnitz, "Bichromatically pumped microresonator frequency combs", *Physical Review A*, vol. 90, no. 1, p. 013 811, 2014.

[104] S. W. Huang, H. Zhou, J. Yang, J. F. McMillan, A. Matsko, M. Yu, D. L. Kwong, L. Maleki, and C. W. Wong, "Mode-locked ultrashort pulse generation from on-chip normal dispersion microresonators", *Physical Review Letters*, vol. 114, no. 5, p. 053 901, 2015.

[105] Y. Liu, Y. Xuan, X. Xue, P.-H. Wang, S. Chen, A. J. Metcalf, J. Wang, D. E. Leaird, M. Qi, and A. M. Weiner, "Investigation of mode coupling in normal-dispersion silicon nitride microresonators for Kerr frequency comb generation", *Optica*, vol. 1, no. 3, pp. 137–144, 2014.

[106] X. Xue, Y. Xuan, P.-H. Wang, Y. Liu, D. E. Leaird, M. Qi, and A. M. Weiner, "Normal-dispersion microcombs enabled by controllable mode interactions", *Laser & Photonics Reviews*, vol. 9, no. 4, pp. L23–L28, 2015.

[107] G. D'Aguanno and C. R. Menyuk, "Nonlinear mode coupling in whispering-gallery-mode resonators", *Physical Review A*, vol. 93, no. 4, p. 043 820, 2016.

[108] P.-H. Wang, F. Ferdous, H. Miao, J. Wang, D. E. Leaird, K. Srinivasan, L. Chen, V. Aksyuk, and A. M. Weiner, "Observation of correlation between route to formation, coherence, noise, and communication per-

formance of Kerr combs", *Optics Express*, vol. 20, no. 28, pp. 29 284–29 295, 2012.

[109] J. Čtyroký, I. Richter, and M. Šiňor, "Dual resonance in a waveguide-coupled ring microresonator", *Optical and Quantum Electronics*, vol. 38, no. 9-11, pp. 781–797, 2007.

[110] L. Yong and A. P. Heberle, "Observation of enhanced group velocity dispersion in coupled waveguide structures", *Journal of Lightwave Technology*, vol. 17, no. 6, pp. 1049–1055, 1999.

[111] M. Soltani, A. Matsko, and L. Maleki, "Enabling arbitrary wavelength frequency combs on chip", *Laser & Photonics Reviews*, vol. 10, no. 1, pp. 158–162, 2016.

[112] S. A. Miller, Y. Okawachi, S. Ramelow, K. Luke, A. Dutt, A. Farsi, A. L. Gaeta, and M. Lipson, "Tunable frequency combs based on dual microring resonators", *Optics Express*, vol. 23, no. 16, p. 21 527, 2015.

[113] A. B. Matsko and L. Maleki, "Feshbach resonances in Kerr frequency combs", *Physical Review A*, vol. 91, no. 1, p. 013 831, 2015.

[114] K. Ikeda, R. E. Saperstein, N. Alic, and Y. Fainman, "Thermal and Kerr nonlinear properties of plasma-deposited silicon nitride/ silicon dioxide waveguides", *Optics Express*, vol. 16, no. 17, pp. 12 987–12 994, 2008.

[115] T. Carmon, L. Yang, and K. J. Vahala, "Dynamical thermal behavior and thermal self-stability of microcavities", *Optics Express*, vol. 12, no. 20, pp. 4742–4750, 2004.

[116] P.-H. Wang, Y. Xuan, L. Fan, L. T. Varghese, J. Wang, Y. Liu, X. Xue, D. E. Leaird, M. Qi, and A. M. Weiner, "Drop-port study of microresonator frequency combs: Power transfer, spectra and time-domain characterization", *Optics Express*, vol. 21, no. 19, pp. 22 441–22 452, 2013.

[117] P.-H. Wang, J. A. Jaramillo-Villegas, Y. Xuan, X. Xue, C. Bao, D. E. Leaird, M. Qi, and A. M. Weiner, "Intracavity characterization of micro-comb generation in the single-soliton regime", *Optics Express*, vol. 24, no. 10, pp. 10 890–10 897, 2016.

[118] X. Xue, Y. Xuan, C. Wang, P.-H. Wang, Y. Liu, B. Niu, D. E. Leaird, M. Qi, and A. M. Weiner, "Thermal tuning of Kerr frequency combs in silicon nitride microring resonators", *Optics Express*, vol. 24, no. 1, pp. 687–698, 2016.

[119] V. Brasch, E. Lucas, J. D. Jost, M. Geiselmann, and T. J. Kippenberg, "Self-referencing of an on-chip soliton Kerr frequency comb without external broadening", *ArXiv e-prints*, p. 1605.02801, 2016.

[120] C. Bao, L. Zhang, A. Matsko, Y. Yan, Z. Zhao, G. Xie, A. M. Agarwal, L. C. Kimerling, J. Michel, L. Maleki, and A. E. Willner, "Nonlinear conversion efficiency in Kerr frequency comb generation", *Optics Letters*, vol. 39, no. 21, pp. 6126–6129, 2014.